SHIFTED BOUNDARY METHOD FOR POISSON PROBLEMS IN LIBMESH

Vinícius da Costa Reis

Dissertação de Mestrado apresentada ao Programa de Pós-graduação em Engenharia Civil, COPPE, da Universidade Federal do Rio de Janeiro, como parte dos requisitos necessários à obtenção do título de Mestre em Engenharia Civil.

Orientador: Alvaro Luiz Gayoso de Azeredo Coutinho

Rio de Janeiro
Outubro de 2019

SHIFTED BOUNDARY METHOD FOR POISSON PROBLEMS IN LIBMESH

Vinícius da Costa Reis

DISSERTAÇÃO SUBMETIDA AO CORPO DOCENTE DO INSTITUTO ALBERTO LUIZ COIMBRA DE PÓS-GRADUAÇÃO E PESQUISA DE ENGENHARIA (COPPE) DA UNIVERSIDADE FEDERAL DO RIO DE JANEIRO COMO PARTE DOS REQUISITOS NECESSÁRIOS PARA A OBTENÇÃO DO GRAU DE MESTRE EM CIÊNCIAS EM ENGENHARIA CIVIL.

Examinada por:

Prof. Alvaro Luiz Gayoso de Azeredo Coutinho, DSc.

Prof. Adriano Maurício de Almeida Côrtes, DSc.

Prof. Renato Nascimento Elias, DSc.

RIO DE JANEIRO, RJ – BRASIL
OUTUBRO DE 2019

Reis, Vinícius da Costa

Shifted Boundary Method for Poisson Problems in libMesh/Vinícius da Costa Reis. – Rio de Janeiro: UFRJ/COPPE, 2019.

X, 44 p.: il.; 29, 7cm.

Orientador: Alvaro Luiz Gayoso de Azeredo Coutinho

Dissertação (mestrado) – UFRJ/COPPE/Programa de Engenharia Civil, 2019.

Referências Bibliográficas: p. 32 – 34.

1. Convergency Analysis. 2. Surrogate Boundary. 3. Immersed Methods. 4. Embedded Methods. 5. Weak Boundary Conditions. 6. libMesh. 7. Finite Elements Methods. 8. Poisson Problem. I. Coutinho, Alvaro Luiz Gayoso de Azeredo. II. Universidade Federal do Rio de Janeiro, COPPE, Programa de Engenharia Civil. III. Título.

To my father.

Resumo da Dissertação apresentada à COPPE/UFRJ como parte dos requisitos necessários para a obtenção do grau de Mestre em Ciências (M.Sc.)

CONTORNO SUBSTITUTIVO PARA PROBLEMAS DE POISSON EM LIBMESH

Vinícius da Costa Reis

Outubro/2019

Orientador: Alvaro Luiz Gayoso de Azeredo Coutinho

Programa: Engenharia Civil

As formulações não conformes do método dos elementos finitos aplicam-se a situações em que malhas conformes têm um custo computacional siginificativo, a ponte de inviabilizar sua avaliação. Nestas a descrição geométrica de um domínio não necessariamente corresponde à descrição geométrica do mapeamento de um contorno físico. Têm o potencial de encurtar a etapa de pré-processamento ao viabilizar a inserção de modelos geométricos analíticos, modelos CAD, sem necessariamente utilizar-se formulações isogeométricas, ou de imagens tomográficas.

Este trabalho apresenta os resultados de uma implementação, utilizando o *framework* libMesh, de uma formulação disponível para problemas de Poisson, referida como Contorno Deslocado. Nesta é definido um contorno substitutivo, conveniente e suficientemente próximo do original, no qual os campos (funções escalares ou vetoriais) são representados por uma expansão de Taylor (de primeira ordem) na região removida. A expansão é então utilizada na composição das condições do novo contorno, que são por fim aplicadas de forma fraca, utilizando-se a abordagem de Nitsche. Dois conjuntos de casos são examinados e seus resultados comparados com suas respectivas soluções analíticas. A taxa de convergência é então avaliada, validando o resultado reportado pelo propositor da formulação.

Abstract of Dissertation presented to COPPE/UFRJ as a partial fulfillment of the requirements for the degree of Master of Science (M.Sc.)

SHIFTED BOUNDARY METHOD FOR POISSON PROBLEMS IN LIBMESH

Vinícius da Costa Reis

October/2019

Advisor: Alvaro Luiz Gayoso de Azeredo Coutinho

Department: Civil Engineering

The non-conformal finite elements formulations applicable to situations in which the computation of conformal meshes are significantly expensive, up to a point where a problem might be redered unfisible.

The embedded finite element method is one approach to diminish the mesh generation burden in finite element analysis. It consists of dealing with a description of a boundary that does not necessarily match the problem's physical boundary. It can potentially shrink the workflow giving the opportunity of immediately inputting a CAD geometry or tomographic image into a simulation, without necessarily using isogeometric elements or performing substantial preprocessing.

This work presents an implementation of the recently proposed embedded formulation for Poisson problems in the general purpose library libMesh. In the formulation, the boundary condition is shifted and enforced weakly by a Nitsche approach, and is referred as Surrogated Boundary. This is accomplished provided the surrogate boundary is close enough to the physical boundary so a Taylor expansion can be used to describe the chopped off region. This approach provides a significant computational relief compared to the alternative of adaptative point integration selection, especially when dealing with complex domains where the total point-locating operations' cost can be significantly high. The reported convergence rate is also examined.

Contents

List of Figures

List of Tables

Chapter 1

Introduction

The unfitted methods is a broad term that encompasses a collection of numerical methods' formulations that are dedicated to solve problems where the mapped geometry of a physical body does not match the contour of the grid or mesh put in place to represent it. Though having its main application in fluid mechanics and fluid structure interaction problems, they are also applicable to other physics.

They are suitable to be used in situations where the mesh generation is such a burden that might even render a problem unsolvable. On the other hand it has been reported [1] that most of the time spent on simulation is on geometry manipulation or mesh generation. As an attempt to cut the intermediate steps between a model conception and its simulation, by adopting B-splines, NURBS or T-splines as base functions, traditionally used as CAD surfaces, the isogeometric formulations is then proposed [2]. An equivalent result might be achieved by using the same functions merely as geometric description in a unfitted method. Regardless on the motivation, whenever geometric manipulation or the mesh generation becomes an issue, either for the manual labor required or the computational cost, the unfitted methods should be considered.

Although frequently used interchangeably, the terms immersed and embedded can be distinguished, separating the unfitted methods in two mains categories. This distinction is made by Main and Scovazzi [3, 4] grouping as immersed the set of formulations that prescribes the discretization of a problem in the entirety of a mesh, that usually is defined as a regular region of the cartesian space, bounding the domain under evaluation and its defining boundary. Conversely the embedded formulations are the ones that removes the elements or cells that are not part of the domain, entirely or, depending on the formulation, partially.

Among the immersed formulations is the pioneer work of Peskin [5] and the level-set methods [6]. On these formulations the enforcement of the boundary condition is done by applying an equivalent force field that can be interpreted as a penalty function.

Within the embedded formulations are the methods derived from the XFEM [7] formulation with boundary condition enforced by Nitsche's method [8]. On this approach, by enriching the approximation space by mean of a discontinuous function it is possible to correctly represent the boundary. The conjunction of the two techniques is examined by Hansbo and Hansbo [9] for a diffusion problem in a discontinuous domain. One of the challenges imposed by this approach is the complexity of correctly detecting the boundary interception in a element.

Still on the embedded category, an interesting approach, designated as Finite Cell Method, is developed for solid mechanics [10] and turbulent flow [11] problems. In this approach the boundary condition representation is achieved by removing elements that lies outside of the geometry under evaluation and also by adopting an adaptive integration scheme on the elements crossed by the boundary. The downside of this technique is the point by point location evaluation, that can be computationally expensive depending on the size of the problem, the number of integration points used and the complexity of the geometry. In its implementation a ray trace algorithm is used, but it is not necessarily the only solution. A review of this method is done by Schillinger [12].

Finally in the embedded set of formulations, grouped in the approximate domain methods, is the Shifted Boundary Method. The boundary condition is shifted and enforced weakly by Nitsche approach, and then referred as surrogated boundary. Its full development and analysis can be found on its original publication [3], here being reported just its final statement. The Nitsche formulation is also implemented as a reference solution and is used to evaluate the quality of the shifted boundary formulation. The surrogate boundary has to be close enough to the true boundary, so that a Taylor expansion can be used to describe the chopped off region.

The implementation is done in the framework libMesh [13] and takes advantage of the subdomain functionality, after geometric evaluations, to segregate the elements crossed by the true boundary, its neighbors inside the domain, composing the surrogate boundary, and the inner and outer elements. The two geometric shapes used to compose the evaluated geometries are circles and spheres.

The remainder of this work is organized as follows. The next section presents briefly the Shifted Boundary Method. Chapter 3 shows the obtained results and the observed convergence for the sets of two and three-dimensional evaluated problems. It then ends with a summary of our main findings and suggestions for future works.

Nitsche's approach was developed in the context of the minimization problem and the application to the finite element method was done by [14].

Chapter 2

Mathematical Formulation and Analysis

In the context of the Finite Element methods an engineering problem is studied by the mathematical branch called Functional Analysis. The properties of a distance function, an intuitive notion lent from the physical world, is used to define what is called a norm $\|\cdot\|$, a real-valued function, over a vector space W, as is presented in appendix A.

An engineering problem can then be abstracted as: Find $u \in W$ such that

$$a(u, v) = f(v), \qquad \forall v \in V, \tag{2.1}$$

where W and V are vector spaces equipped with its own norms, a is a continuous bilinear form on $W \times V$, and f is a continuous linear form on V. W is called the solution space and V is called the test or trial space. Both spaces are assumed as Hilbert or Banach spaces.

By the definition proposed by Hadamard [15], a problem is well posed if it admits a unique solution and is stable, meaning the solution is controlled by the data in some norm. Two important results are usually used to assert well-posedness, the Lax-Milgram Lemma and the Banach-Nečas-Babuška theorem, presented in appendix A. The first is a sufficient condition for well-posedness and the second gives the necessary and sufficient condition.

Moreover, the formulation of a bilinear form is a craft, and not always the introduction of an additive term can be directly explained. Frequently it is an iterative process between a proposition and the desirable properties verification. Any term addition is licit provided it is demonstrated the added residues can be controlled and is bounded by the adopted norm defined on that space. This of course comes with the price of possibly penalizing the convergence which should always be kept in mind.

The symmetry of a bilinear form is also a desirable property. It can be used to assist a norm elaboration, sometimes being the norm itself, and further on, in the numerical implementation, it leads to a symmetric numerical system to be solve.

The selected problem is restricted to the classical Poisson equation, which is the diffusive term of the complete transport equation. Although not being a challenge in itself, the problem is sufficient to test the reported properties of the examined formulation and to motivate its exploratory implementation.

The Shifted Boundary Formulation is built upon Nitsche's formulation and both development are succinctly described hereafter. The consistency, continuity and coercivity are shown in appendix B.

2.1 Nitsche's Formulation

The problem's statement in its strong form, is: find the solution $u \in C^2(\Omega)$ such that

$$\begin{aligned} -\triangle u &= f, && \text{on} \quad \Omega \\ u &= u_D, && \text{on} \quad \Gamma_D = \partial\Omega, \end{aligned} \tag{2.2}$$

were $\triangle$ is the Laplace operator, u the scalar field to be found, f the source term, Ω a bounded open domain, and Γ_D the boundary where Dirichlet condition u_D is prescribed. This statement is referred as strong because the smoothness requirement is of the same order as the maximum order of its differential operator.

For the sake of notation simplification the integral operators,

$$(v, w)_\omega = \int_\omega vw d\omega \qquad \text{and} \qquad (\mathbf{v}, \mathbf{w})_\omega = \int_\omega \mathbf{v} \cdot \mathbf{w} d\omega \tag{2.3}$$

are defined respectively for scalar and vector operands in a generic domain ω. And its analogous operators,

$$\langle v, w \rangle_\gamma = \int_\gamma vw d\gamma \qquad \text{and} \qquad \langle \mathbf{v}, \mathbf{w} \rangle_\gamma = \int_\gamma \mathbf{v} \cdot \mathbf{w} d\gamma, \tag{2.4}$$

are defined for a subset of these domain's boundary. The operators are bilinear, as one can immediately verify, greatly simplifying the performed equation handling. Naturally the resulting operand should be square integrable and thus restricted to the L^2 space.

The weak formulation of the problem defined in equation 2.2 can be written as,

$$(\nabla v, \nabla u) - \langle v, \nabla u \cdot \mathbf{n} \rangle_{\Gamma_D = \partial\Omega} = (v, f)_\Omega \tag{2.5}$$

where v is the trial function, and $\mathbf{n}$ is the outward pointing normal. The continuity

requirements for this statement is weakened such that the solution space is assumed as $u \in H^1(\Omega)$ and the trial space $v \in H^1_{0,D}(\Omega)$. The classical Galerkin formulation corresponds to this statement when the approximation spaces and the trial spaces are finite-dimensional being denoted as $V^h(\Omega) \subset H^1(\Omega)$. The nomenclature for the respective functions is then assumed as u^h and w^h, where h is the characteristic length of the space partition, which in the context of finite elements is the mesh. An analysis of this problem can be found in [16].

A further relaxation of the problem is achieved in Nitsche's formulation by assuming the same space for u and v, meaning now $v \in H^1(\Omega)$ as well, and by adding the two residues,

$$\begin{aligned} &- \langle \nabla v \cdot \mathbf{n}, u - u_D \rangle_{\Gamma_D} \\ &+ \eta \langle v, u - u_D \rangle_{\Gamma_D} , \end{aligned} \tag{2.6}$$

where η is the penalization parameter, and its value is reported further on.

The first term, introduces a variation to the boundary condition that is now approximately complied, whilst still maintaining consistency, and the second guarantees the coercivity of the respective bilinear form.

The formal statement, already in the finite dimensional space, is then: Find $u^h \in V^h(\Omega)$ such that, $\forall v \in V^h$,

$$\begin{aligned} &\left(\nabla v^h, \nabla u^h\right) - \left\langle v^h, \nabla u^h \cdot \mathbf{n} \right\rangle_{\Gamma_D} - \left\langle \nabla v^h \cdot \mathbf{n}, u^h - u_D \right\rangle_{\Gamma_D} \\ &+ \eta \left\langle v^h, u^h - u_D \right\rangle_{\Gamma_D} = \left(v^h, f\right)_{\Omega} . \end{aligned} \tag{2.7}$$

This is the formulation implemented and used as reference, along with some specific analytical solutions.

2.2 The Shifted Boundary Formulation

The formulation development starts by defining a surrogate domain $\tilde{\Omega}$ bounded by $\tilde{\Gamma}$, the surrogate boundary. The relation $(\tilde{\Omega} \cup \tilde{\Gamma}) \subset \Omega$ holds and $\mathbf{d}$, defined bellow, is the displacement vector between the surrogate and the true boundary. Any surrogate boundary related quantity is then annotated with an over tild as illustrated in figure 2.1.

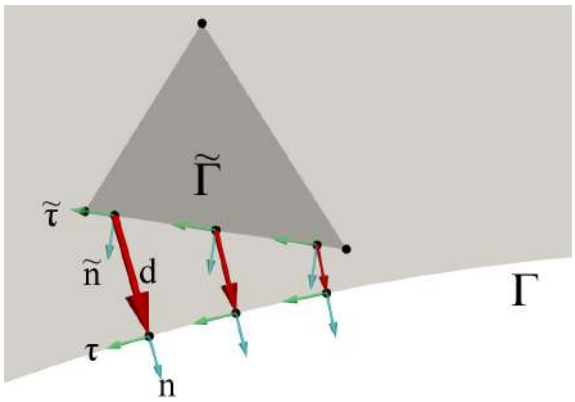

Figure 2.1: True and surrogate boundary with normal, tangent and displacement vector.

The definition of a map function between the surrogate boundary and the original one,

$$\begin{aligned} \mathbf{M} : &\widetilde{\Gamma} \to \Gamma \\ &\widetilde{\mathbf{x}} \mapsto \mathbf{x} \end{aligned} \tag{2.8}$$

is necessary so that any quantity can be shifted from one to the other, and properly taken into account in the new domain. These quantities are refereed as extension. The extension of an arbitrary function ψ defined on Γ can then be defined on $\widetilde{\Gamma}$ as

$$\overline{\psi}\left(\widetilde{\mathbf{x}}\right) \equiv \psi\left(\mathbf{M}\left(\widetilde{\mathbf{x}}\right)\right). \tag{2.9}$$

For the simple geometries evaluated in this work the closest distance from $\widetilde{\Gamma}$ to Γ, is the natural mapping choice, and, as a beneficial consequence, the displacement vector is aligned with the mapped true normal.

The shifted unitary normal vector is then defined as

$$\overline{\mathbf{n}}\left(\widetilde{\mathbf{x}}\right) \equiv \mathbf{n}\left(\mathbf{M}\left(\widetilde{\mathbf{x}}\right)\right), \tag{2.10}$$

and the displacement vector $\mathbf{d}$ as

$$\mathbf{d} = \mathbf{M}\left(\widetilde{\mathbf{x}}\right) - \widetilde{\mathbf{x}}, \tag{2.11}$$

which are both independent of the chosen mapping function.

Building upon the previews definitions, it is then possible to evaluate the Taylor expansion centered at a point of the surrogate boundary, i.e. for $\widetilde{\mathbf{x}} \in \widetilde{\Gamma}_D$ as

$$\begin{aligned} u\left(x\right) = u\left(\mathbf{M}\left(\widetilde{\mathbf{x}}\right)\right) = \overline{u}_D\left(\widetilde{\mathbf{x}}\right) &= u\left(\widetilde{\mathbf{x}}\right) + \nabla u\left(\widetilde{\mathbf{x}}\right) \cdot \left(\mathbf{x} - \widetilde{\mathbf{x}}\right) + O\left(||\mathbf{x} - \widetilde{\mathbf{x}}||^2\right) \\ 0 &= u\left(\widetilde{\mathbf{x}}\right) + \nabla u\left(\widetilde{\mathbf{x}}\right) \cdot \left(\mathbf{x} - \widetilde{\mathbf{x}}\right) - \overline{u}_D\left(\widetilde{\mathbf{x}}\right) + O\left(||\mathbf{x} - \widetilde{\mathbf{x}}||^2\right) \end{aligned} \tag{2.12}$$

The equivalent shifted boundary condition is assumed to be a truncated Taylor expansion, which in practice is a linear approximation, that introduces a second order error, and is as good as the distance between the two boundaries.

By taking the weak statement (equation 2.5) an equivalent formulation can be achieved by adding two mutual canceling terms,

$$(\nabla v, \nabla u)_{\Omega} - \langle v, \nabla u \cdot \mathbf{n} \rangle_{\Gamma_D} - \langle \nabla v \cdot \mathbf{d}, \nabla u \cdot \mathbf{n} \rangle_{\Gamma_D} + \langle \nabla v \cdot \mathbf{d}, \nabla u \cdot \mathbf{n} \rangle_{\Gamma_D} = (v, f)_{\Omega} \quad (2.13)$$

which in turn, by adding the two Nitche's terms (equation 2.6) and by applying the Taylor expansion (equation 2.12) on them, for both u and v, then gives,

$$\begin{aligned} &(\nabla v, \nabla u)_{\widetilde{\Omega}} - \langle v, \nabla u \cdot \mathbf{n} \rangle_{\widetilde{\Gamma}_D} - \langle \nabla v \cdot \mathbf{d}, \nabla u \cdot \mathbf{n} \rangle_{\widetilde{\Gamma}_D} \\ &+ \langle \nabla v \cdot \mathbf{d}, \nabla u \cdot \widetilde{\mathbf{n}} \rangle_{\widetilde{\Gamma}_D} - \langle \nabla v \cdot \mathbf{n}, u + \nabla u \cdot \mathbf{d} - u_D \rangle_{\widetilde{\Gamma}_D} \\ &+ \eta \langle v + \nabla v \cdot \mathbf{d}, u + \nabla u \cdot \mathbf{d} - u_D \rangle_{\widetilde{\Gamma}_D} = (v, f)_{\widetilde{\Omega}}, \end{aligned} \quad (2.14)$$

where the $\overline{u}_D$ notation is simplified to u_D with no loss in clarity. By doing this, effectively the unfitted boundary condition is further perturbed by the added gradients.

By using the decomposition,

$$\nabla u^h \cdot \tilde{\mathbf{n}} = \frac{(\mathbf{n} \cdot \tilde{\mathbf{n}})}{\|\mathbf{d}\|} \nabla u^h \cdot \mathbf{d} + \left(\nabla u^h \cdot \tau_i \right) \tau_i \cdot \tilde{\mathbf{n}} \quad (2.15)$$

and the approximation

$$\nabla u^h \cdot \tau_i \approx \nabla \overline{u}_D \cdot \tau_i \quad (2.16)$$

the problem can then be stated as

$$\begin{aligned} &(\nabla v, \nabla u)_{\widetilde{\Omega}} - \langle v + \nabla v \cdot \mathbf{d}, \nabla u \cdot \widetilde{\mathbf{n}} \rangle_{\widetilde{\Gamma}_D} \\ &+ \left\langle \nabla v \cdot \mathbf{d}, \frac{(\mathbf{n} \cdot \tilde{\mathbf{n}})}{\|\mathbf{d}\|} \nabla u \cdot \mathbf{d} + (\nabla \overline{u}_D \cdot \tau_i) \tau_i \cdot \widetilde{\mathbf{n}} \right\rangle_{\widetilde{\Gamma}_D} \\ &- \langle \nabla v \cdot \widetilde{\mathbf{n}}, u + \nabla u \cdot \mathbf{d} - \overline{u}_D \rangle_{\widetilde{\Gamma}_D} \\ &+ \eta \langle v + \nabla v \cdot \mathbf{d}, u + \nabla u \cdot \mathbf{d} - \overline{u}_D \rangle_{\widetilde{\Gamma}_D} = (v, f)_{\widetilde{\Omega}} \end{aligned} \quad (2.17)$$

Which finally leads its formal statement: Given the discrete subspace $V^h(\Omega) \subset H^1(\Omega)$, where V^h is the space of piecewise continuous functions (typically of polynomial base) find $u^h \in V^h(\Omega)$, such that $\forall w^h \in V^h(\Omega)$,

$$a^h\left(u^h, v^h\right) = l^h\left(v^h\right)$$

$$\begin{aligned} a^h\left(u^h, v^h\right) = & \left(\nabla v^h, \nabla u^h\right)_{\widetilde{\Omega}} - \left\langle v^h + \nabla v^h \cdot \mathbf{d}, \nabla u^h \cdot \mathbf{n}\right\rangle_{\tilde{\Gamma}_D} \\ & - \left\langle \nabla v^h \cdot \mathbf{n}, u^h + \nabla u^h \cdot \mathbf{d}\right\rangle_{\tilde{\Gamma}_D} + \left\langle \nabla v^h \cdot \mathbf{d}, \frac{(\mathbf{n} \cdot \tilde{\mathbf{n}})}{\|\mathbf{d}\|} \nabla u^h \cdot \mathbf{d}\right\rangle_{\tilde{\Gamma}_D} \\ & + \eta \left\langle v^h + \nabla v^h \cdot \mathbf{d}, u^h + \nabla u^h \cdot \mathbf{d}\right\rangle_{\tilde{\Gamma}_D} \end{aligned} \tag{2.18}$$

$$\begin{aligned} l^h\left(w^h\right) = & \left(v^h, f\right)_{\tilde{\Omega}} - \left\langle \nabla v^h \cdot \tilde{\mathbf{n}}, \overline{u}_D\right\rangle_{\tilde{\Gamma}_D} \\ & - \left\langle \nabla v^h \cdot \mathbf{d}, \left(\nabla u_D \cdot \tau_i\right) \tau_i \cdot \tilde{\mathbf{n}}\right\rangle_{\tilde{\Gamma}_D} + \eta \left\langle v^h + \nabla v^h \cdot \mathbf{d}, \overline{u}_d\right\rangle_{\tilde{\Gamma}_D} \end{aligned}$$

The penalization parameter η is defined as $\frac{\alpha}{h^{\perp}}$ where $h^{\perp}$ is the perpendicular characteristic length and the used α is the estimation taken as $\alpha = 5(p+1)$ where p is the order of the polynomial base of the approximation space, which for the first order elements used in this work is taken as $\alpha = 10$.

The proved analytical convergence rate by Main and Scovazzi [3] is of order 1.5, but the original publication also reports optimal second-order convergence rate in their numerical experiments, leaving open the speculation that the proved rate might be a lower bound and liable to sharper estimations.

Chapter 3

Numerical Implementation

The current chapter describes how the standard libMesh workflows is adapted so the Surrogate Boundary can be implemented. It does not intend to show in detail how the implementation works, but rather serve as a guideline to reproduce the work. For a detailed description on libMesh classes, it is recommended to check its documentation and source code [17]. It also describes how the geometry is handled, in this case the purpose is to serve as a baseline for the discussion in the Conclusion and Future Works chapter, and its value relies more on the insight it provokes than in the implementation itself.

3.1 libMesh implementation

Although flexible, the basic work flow generally implemented in libMesh is presented in figure 3.1. The particular parts which are specific to the Surrogate Boundary are colored in yellow, and is better detailed further on.

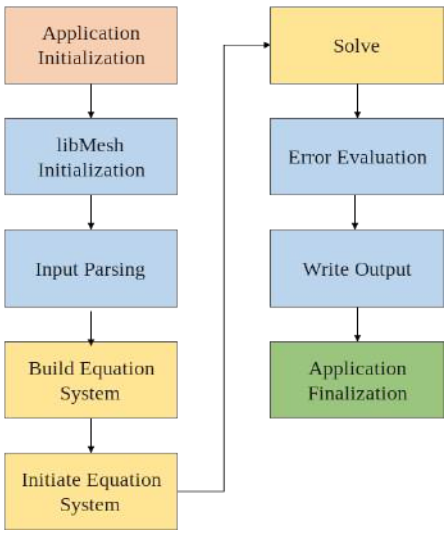

Figure 3.1: Basic libMesh flowchart.

The execution begins by evaluating the command line input that is basically a path to a file in which all the model information is referenced. This file, besides some meta-model-information, points to a set of files containing the mesh to be used (conformal or a background), and a set of files that describes the geometry. Each shape has an equivalent implemented class to which the input parsing is delegated. This is done so the geometry management is abstracted out from the main program workflow.

Besides the input handling, other aspects like parsing if a node is inside or outside, or if an element is inside, crossed by or outside the geometry, the distance and projection of a point onto a geometry, normals and tangents vectors evaluation, and the associated boundary condition (Neumman or Dirichlet), and, when available, the analytical solution, are also implemented in the geometry class.

As an illustration, the representation of a spherical shell or an annulus can be done with only one geometry class, by excluding the interior and including the exterior of the smaller sphere or circle, and by inverting the selection in the bigger ones. This seminal implementation of a boolean operation onto a B-rep (boundary representation) of a solid model is scalable and can be qualified, by adopting the jargon, embarrassingly parallel. The only synchronization point would be the final geometry composition where the distance, projection point, normal and tangents vectors, or any other necessary quantity, would have to be selected out among all its respective basic geometric shape. Each quantity is a parallelization problem in itself and its implementation should be judiciously evaluated for the target architecture.

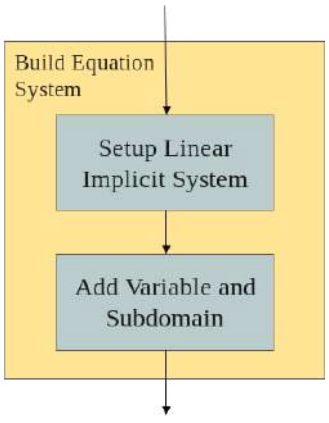

Figure 3.2: Building equation system detailed.

At the system building phase, a variable and its subdomains are simultaneously added to a system, as illustrated in figure 3.2. At this point the added variable is implicitly associated to a subdomain list. For the proposed formulation only two subdomains are necessary for each physics, one for the inner element and the other for the surrogate boundary elements. For coupling two domains, as in a multi-physics approach, another set of disjoint subdomains also would have to be defined.

Before assembling the equation system, an implicit call to an initialization method is performed. At this point the element's subdomain evaluation is done, by using the basic geometry class which was described before. The initialization method is shown in figure 3.3 and is one of the critical sessions in the implementation, meaning albeit exploratory, a significant amount of execution time is spent at this stage.

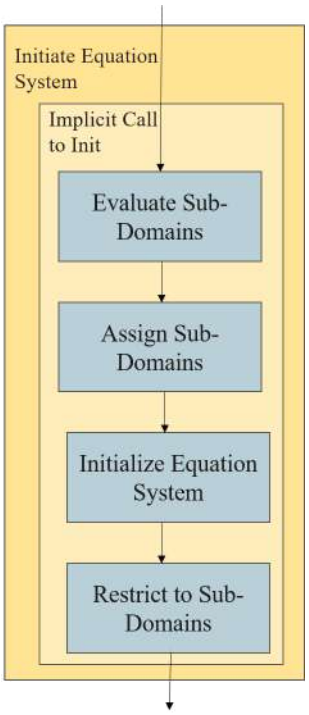

Figure 3.3: Equation system initialization.

The call to restrict the solver to an specific subdomain list is implemented by the framework, and is where the non used degrees of freedom are removed from the equation system. The attempt to use the adaptive mesh refinement infrastructure offered by the framework was done at this point by both calling the routine in between refinements and at the end of a set of refinement iterations. Regardless of the initialization parameter used [17] the execution was dropped by an unhandled exception. This is further explained in chapter 5.

The equation system assemblage is also implicitly done and is the formulation's core, where the equation system is effectively built. This is done by using the iterators offered by the framework which are automatically available for the entire mesh and the applied subdomains. The elements evaluation is firstly done for the inner elements and then for the surrogate ones. This phase is depicted in figure 3.4 and the expression "regular term" refers to the terms present in both inner and surrogate elements. The calculation is split just as a mean to rationalize the implementation, and was not done having optimization as the main objective.

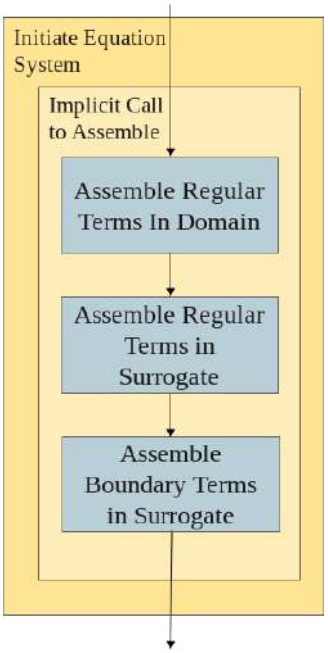

Figure 3.4: Equation system assemblage.

The remaining operations shown in the diagram depicted in figure 3.1 have no specific implementation for the surrogate boundary formulation and so they are not described here, the framework documentation is enough to reproduce the implementation. The only specific detail left is the error evaluation that is done by calling the analytical solution for the tested cases, and are found in appendix C. This evaluation is done internally by the framework and is performed at the integration points, as described on chapter 4.

3.2 Geometry Evaluation

The basic geometric quantities necessary for the element matrix evaluation are similarly evaluated for the 2D and the 3D models, and its basic components are illustrated in figure 3.5.

The mapping of a point $\widetilde{\mathbf{x}}$ in the surrogate boundary to a point $\mathbf{x}$ in the original boundary is made by stretching the vector $d_{C,\widetilde{\mathbf{x}}}$ onto the original boundary so the displacement can be evaluated. By defining $\mathbf{d}_{C,\widetilde{\mathbf{x}}} = \widetilde{\mathbf{x}} - \mathbf{C}$, were $\mathbf{C}$ is the center of the circle or sphere, the displacement from the surrogate boundary to the original one is evaluated as

$$\mathbf{d} = \mathbf{d}_{C,\widetilde{\mathbf{x}}} \left(\frac{r}{\| \mathbf{d}_{C,\widetilde{\mathbf{x}}} \|} - 1 \right). \tag{3.1}$$

The normal vector is co-linear to $\mathbf{d}_{C,\widetilde{\mathbf{x}}}$ and can be trivially evaluated by normalizing the later.

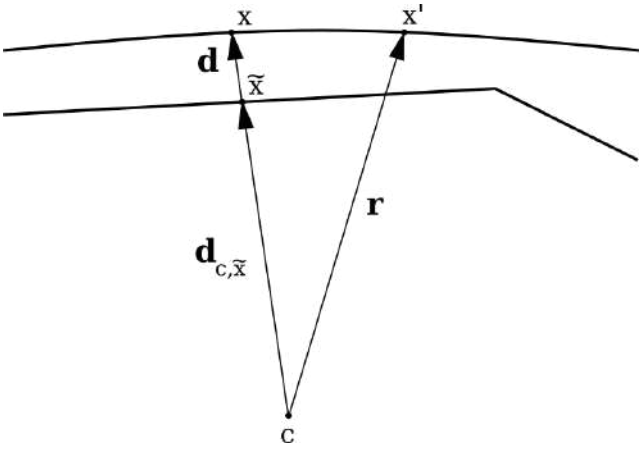

Figure 3.5: Geometric evaluation.

As for the tangent vector, in the two-dimensional case, it is the result of the cross product of the normal vector **n** with a vector perpendicular to the plane in which the problem is defined. For the three-dimensional case an artifice is used so they can be uniquely defined, first a modified normal vector is introduced by changing the original's coordinate order, say for each

$$n^T = \{n_1, n_2, n_3\}$$

we have

$$n_m^T = \{n_2, n_1, n_3\}.$$

This guarantees that both vector are never co-linear. The first tangent vector is then evaluated as

$$\tau_1 = n \times n_m$$

and the second as

$$\tau_2 = \tau_1 \times n.$$

Although trivial, these evaluations are made for every integration point and so have a significant weight in the execution time.

Chapter 4

Results

Two sets of cases are evaluated for both implemented formulations: Nitsche's and the Shifted Boundary. The first set comprises of six conformal meshes representing an annular geometry and six two-dimensional background meshes of equivalent element size. For the second set, five conformal meshes representing a spherical shell and five equivalent three-dimensional background meshes as well. Both cases are identically defined, as shown in table 4.1, where r_e is the external radius, r_i the inner radius, u_e the prescribed Dirichlet boundary condition in the external circle or sphere, u_i in the inner circle or sphere, and f the source term, as defined before. The similarity of both cases is kept only for convenience.

Table 4.1: Annulus and Spherical Shell definition.

Properties	
$u_i = 34$	$r_i = 0.5$
$u_e = 13$	$r_e = 1.0$
$f = 0$	

The meshes are increasingly denser so that the accuracy of the solution can be compared. The error evaluation is performed for all cases by projecting the analytical solution onto the evaluated mesh, case by case. By doing this the comparison is performed in the same solution space available for the space partition under evaluation, leaving only error component perpendicular to it. The L^2 and H^1 error norms are evaluated for every group case and plotted in a graph where its convergence rate can be inferred. Its suitability as a global quality measure of an approximation is discussed later on chapter 5.

A regular mesh would be the first option to be used with the surrogate boundary formulation, or even, with any other embedded formulations, mainly for its ease of generation. Nevertheless, as the comparison with conformal meshes is intended, and the mesh generators publicly available are easy enough to be used with simple ge-

ometries, adopting unstructured meshes in both cases do not adds much complexity to the work and introduces no loss in the intended evaluation.

Finally, the chosen cases are simple enough so its analytical solution can be evaluated as reference, but they are sufficient to infer the convergence rate of the evaluated method.

4.1 Annulus evaluation

As for the annulus geometry, the six conformal meshes is shown in figure 4.1. The images shows increasingly denser meshes and gives an insight on the magnitude of the change in the average element size, up to a point where it is not possible to distinguish the elements in the presented scale. For the mesh generation the maximum and minimum heights are limited to a range, guaranteeing an homogeneous distribution and good ratio factor for the elements.

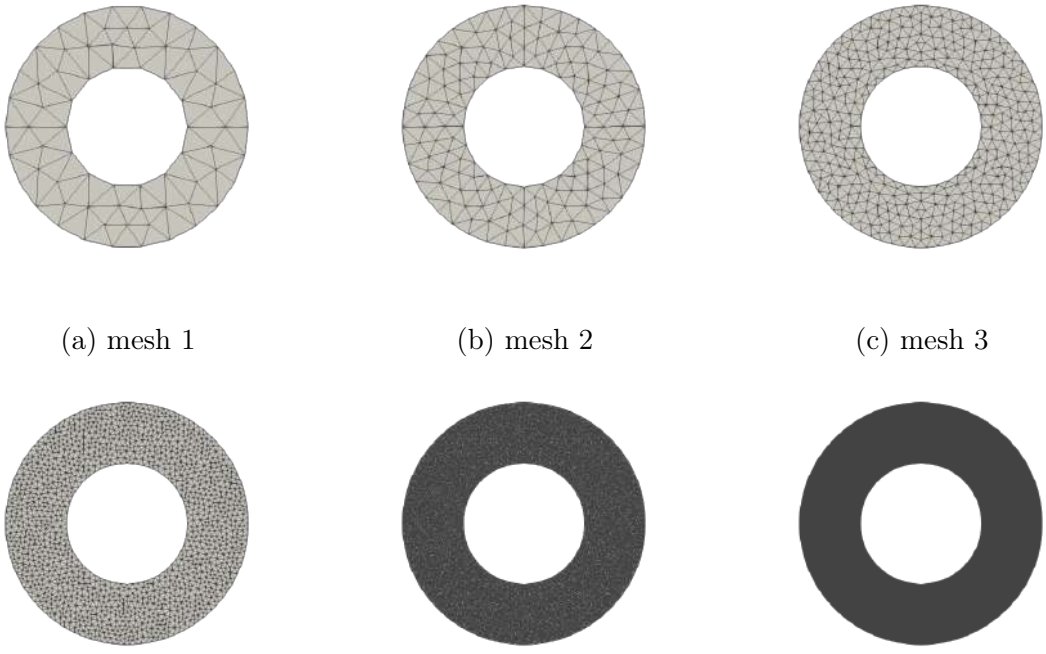

(a) mesh 1 (b) mesh 2 (c) mesh 3

(d) mesh 4 (e) mesh 5 (f) mesh 6

Figure 4.1: Annular domain, conformal meshes.

The equivalent set of background meshes used with the Shifted Boundary formulation is shown in Figure 4.2. For each case, the average element size approximately matches its conformal pair. The images do not highlight the edges of the elements, but they can be distinguished by its color. The depicted colors group the elements according to their classification, being red the elements crossed by the boundary

and so, removed from the problem; light blue, the elements inside the domain; and light pink the elements inside the domain neighboring the removed ones. This last group composes the surrogate boundary and are the only elements in which the formulation specific terms is calculated. The circumference of the original boundary is superposed, in white, and can be promptly noted in the first four cases.

The dark blue elements are all removed from the problem, and they are a display of how much an adaptive mesh refinement, equipped with some geometric criterion, can rationalize computational resources. An attempt to implement it in the adopted framework version was done, but a necessary unimplemented feature rendered it impossible. Adapting the framework itself would then be necessary, more on this in the conclusion chapter.

From these images it is possible to notice how the surrogate domain gradually converges to the desired geometry. This is referenced as geometry conversion, and is measured as the ratio between the area of both domains $A(\widetilde{\Omega})/A(\Omega)$. It is also possible to notice that, since the surrogate domain area never reaches the original domain, the measure of the red elements is a good hint of the asymptotic error .

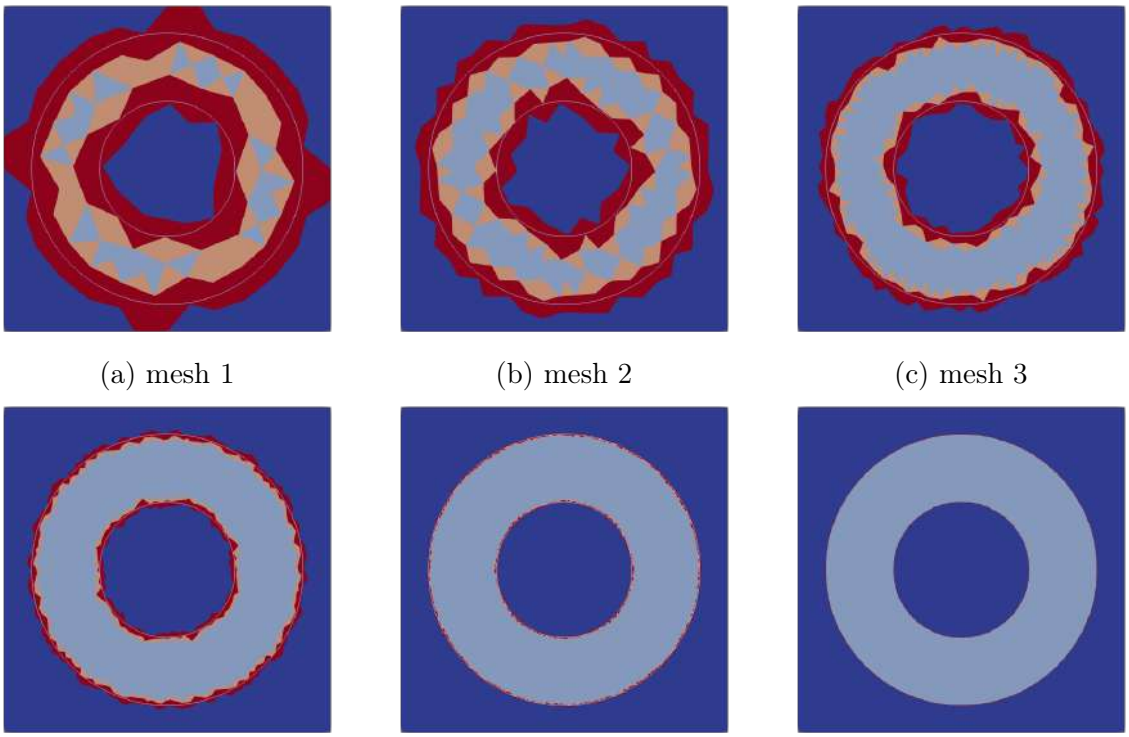

(a) mesh 1 (b) mesh 2 (c) mesh 3

(d) mesh 4 (e) mesh 5 (f) mesh 6

Figure 4.2: Subdomain evaluation, annular domain.

The resulting scalar field for the conformal cases can be seen in Figure 4.3. The mesh is not highlighted because in the denser cases it would prevent from visualizing the solutions, nevertheless the increasing resolution can be noted by the boundary shape. It is possible to notice the quick convergence when from case 3 onward, no

significant difference can be noticed. The convergence to the expected distribution is shown further on. Generally, for an engineering purpose, this would already be a good enough result, but since the objective is to generate more data points to be analyzed the simulation is performed through out all the proposed meshes.

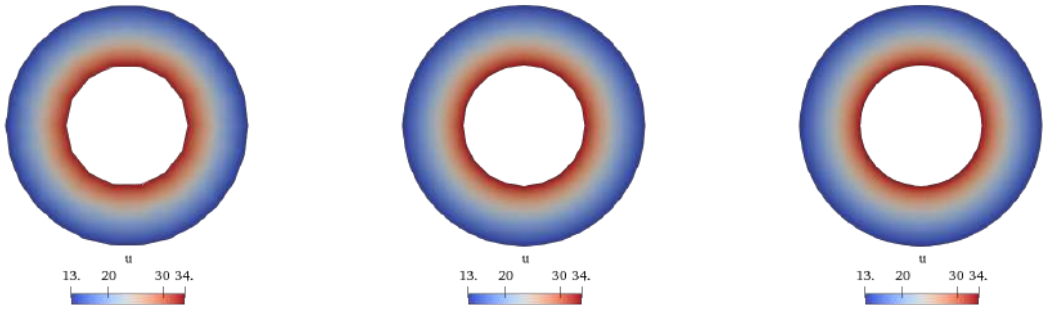

(a) mesh 1 (b) mesh 2 (c) mesh 3

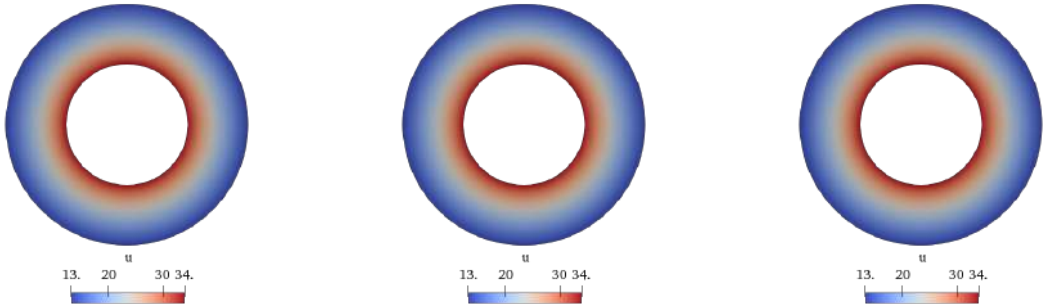

(d) mesh 4 (e) mesh 5 (f) mesh 6

Figure 4.3: Resulting field for the conformal formulation, annular domain.

The resulting scalar field for the Shifted Boundary formulation can be seen in Figure 4.4, where it is possible to notice the immediate alike distribution even on the courser cases. At the surrogate boundary it is also possible to see along its jagged facets the tendency to match the resulting distribution in the equivalent region of the original domain, indicating the proposed boundary approximation is appropriate. Two circles are plotted as reference, they represent the original domain contour. The approximate solution convergence increases along with the geometric convergence.

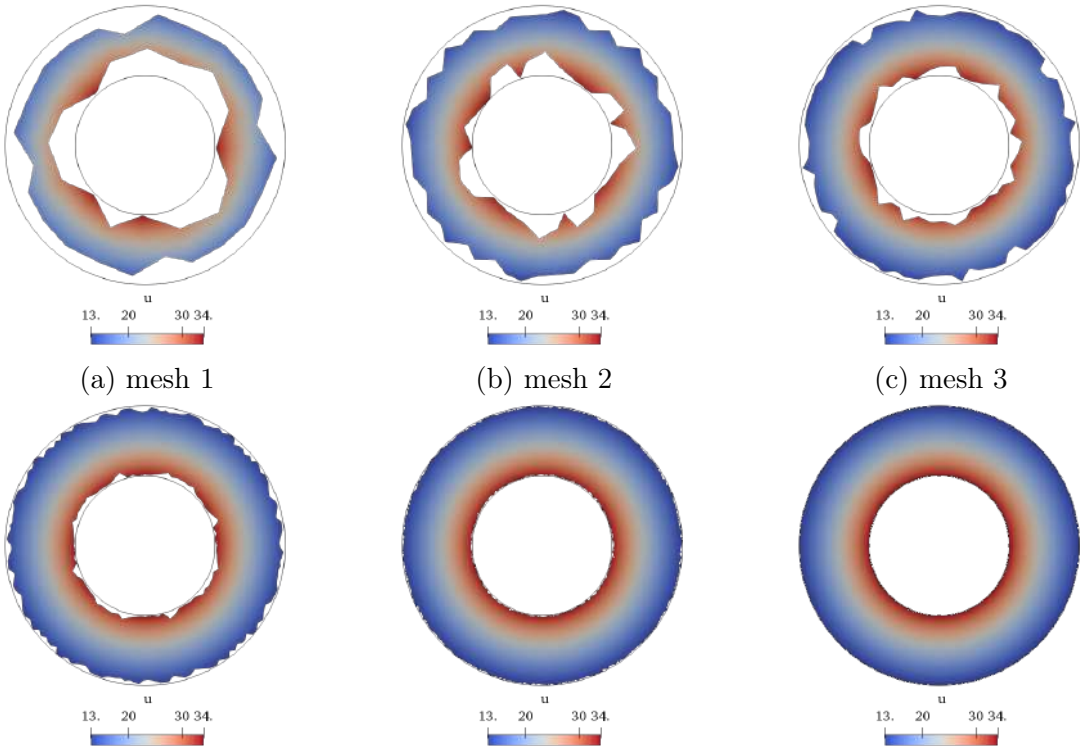

(a) mesh 1 (b) mesh 2 (c) mesh 3

(d) mesh 4 (e) mesh 5 (f) mesh 6

Figure 4.4: Shifted boundary formulation, annular domain.

The analytical solution used as the reference for every error evaluation presented in the following is

$$u\left(r(\mathbf{x})\right) = (u_i - u_e)\frac{\ln\left({}^{r(\mathbf{x})}/_{r_e}\right)}{\ln\left({}^{r_i}/_{r_e}\right)} + u_e, \tag{4.1}$$

where, $r(\mathbf{x}) = (x^2 + y^2)^{\frac{1}{2}}$, and its gradient is

$$\nabla u(\mathbf{x}) = (u_i - u_e)\frac{r_e}{\ln\left({}^{r_i}/_{r_e}\right)}\frac{1}{(x^2+y^2)}\begin{Bmatrix} x \\ y \end{Bmatrix}. \tag{4.2}$$

Its full development can be found in Appendix C.

The relative error evaluation, depicted in figure 4.5, was performed in the post-processing phase by applying the analytical solution as nodal data, effectively representing its projection to the adopted mesh. This approach is subtly different from the error norms evaluation which is performed in the simulation phase, and the analytical solution is evaluated in the integration point. Nevertheless the error plot is useful as a qualitative picture of the error distribution.

The result has a quite homogeneous error distribution, with its maximum values, ranging from 10^{-2} down to 10^{-6}, concentrated around the boundaries. This error feature can be explained firstly due to the geometric conversion, since rectilinear edges of an element needs to be small enough to fit the proposed geometry, and

secondly due the non-consistent nature of Nitsche's formulation. Nevertheless the results are as good as expected, and, generally, for an engineering purpose, correct. These features are highlighted only for comparison reasons.

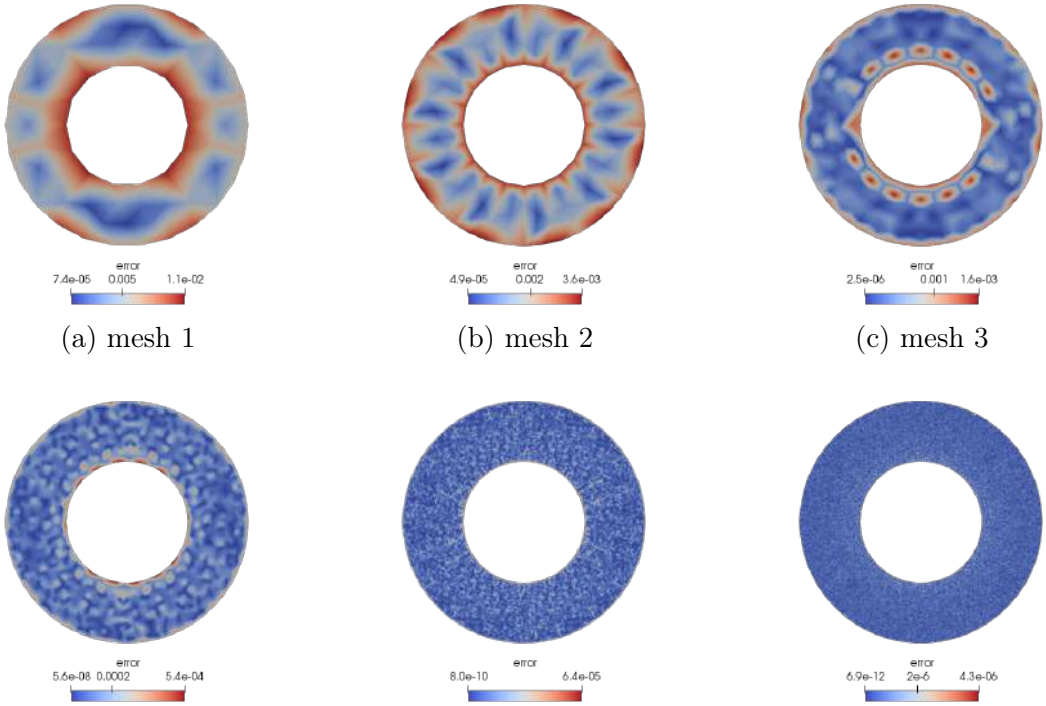

(a) mesh 1 (b) mesh 2 (c) mesh 3

(d) mesh 4 (e) mesh 5 (f) mesh 6

Figure 4.5: Relative error on conformal formulation, smaller annular domain.

As for the relative error in the Shifted Boundary formulation, the error has also an homogeneous distribution characteristics, as good as the substitutive mesh approximation, ranging from 10^{-2} down to 10^{-5}. Its maximum is also closer to the boundary, in this case due to the linear approximation introduced.

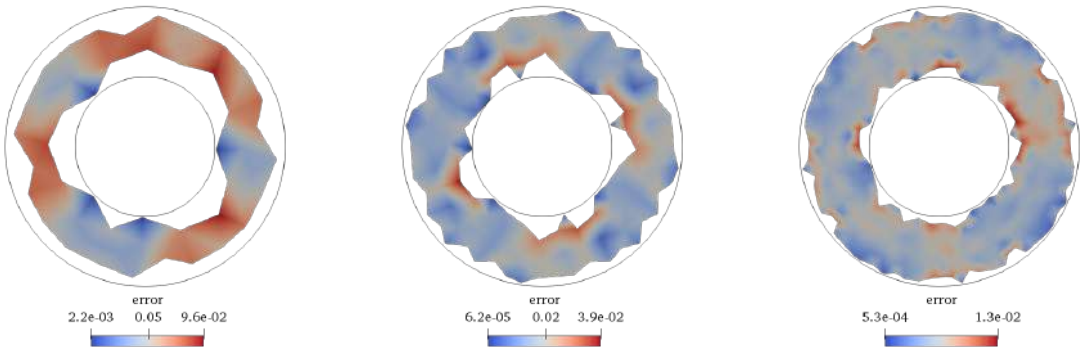

(a) mesh 1 (b) mesh 2 (c) mesh 3

Figure 4.6: Relative error on shifted boundary formulation, annular domain (continue).

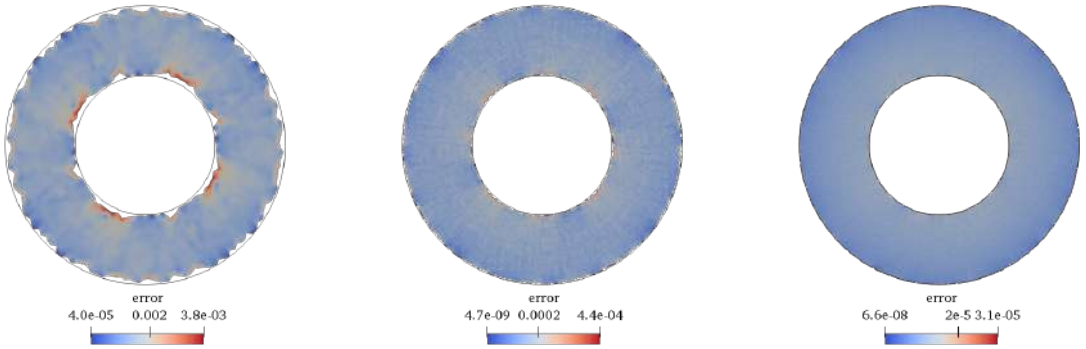

(d) mesh 4 (e) mesh 5 (f) mesh 6

Figure 4.6: Relative error on shifted boundary formulation, annular domain.

The radial sampling of the resulting scalar field can be seen in Figure 4.7a for the conformal formulation and in 4.7b for the Shifted Boundary. The effect of the geometric convergence can be noticed, in the conformal cases, by the spread of the prescribed boundary value at the radius extremes, i.e. $r = 0.5$ and $r = 1.0$, and in the Shifted Boundary cases by the valueless chopped off region, just as expected. Nevertheless quick conversion can be noticed in both cases, and the results begins to get indistinguishable, aside from the removed region, from the third mesh refinement onward. The analytical solution is plotted in red, in both graphs, and can not be distinguished in the line clutter of the denser meshes' results.

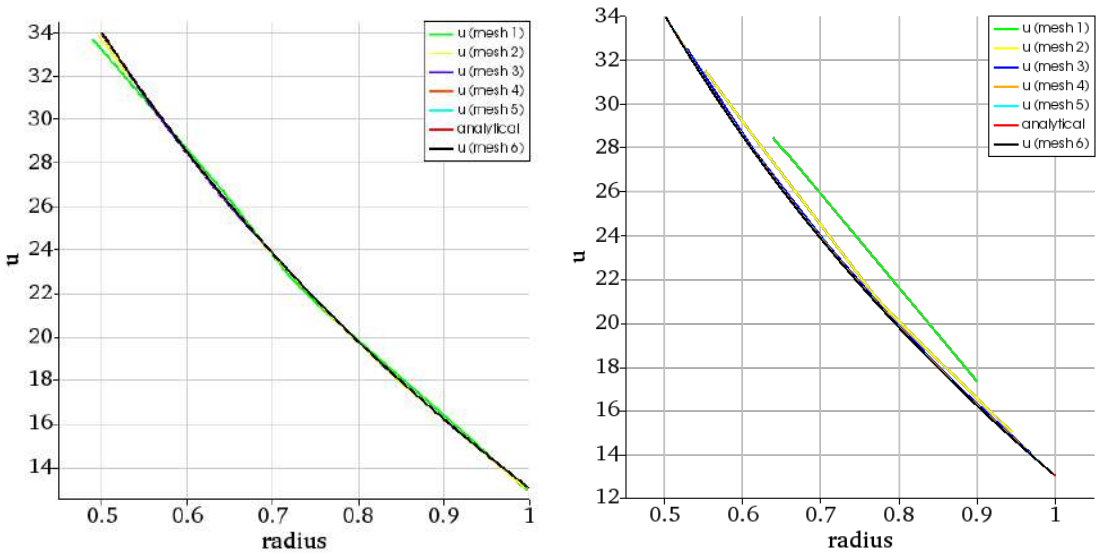

(a) Conformal (b) Shifted Boundary

Figure 4.7: Radial sampling of u and u^h on annular domain.

The resulting L^2 error norm is plotted in logarithmic scale in Figure 4.8. The conformal formulation is shown in green and the Shifted Boundary formulation, refereed as embedded, is show in blue. It is possible to notice a similar slope on both adjusted lines, and indeed, the resulting coefficients indicates a second order

convergence for both of them. It is also possible to notice that the two lines are approximately parallels but not co-linear, this is due to the asymptotic characteristic of the Shifted Boundary formulation.

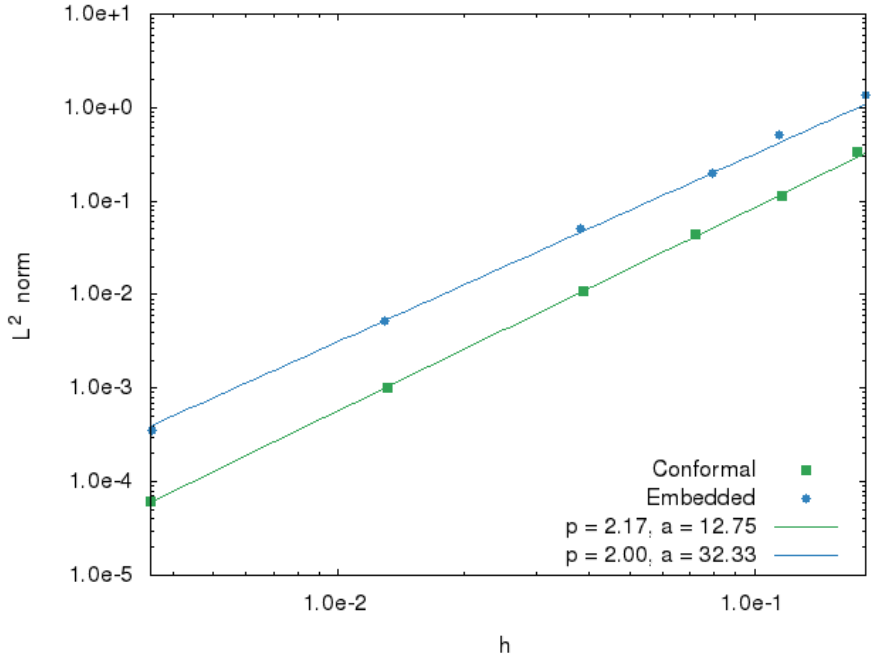

Figure 4.8: L^2 error norms on annular domain.

The same arrangement is done for the H^1 error norm, displayed in Figure 4.9, log scale, colors arrangement and linear regressions were performed in the same manner. The first order convergence rate is compatible with the obtained results for the L^2 norm, additionally an approximate co-linearity for both formulations' results was observed.

The linear regression adjusts the data to the curve,

$$y = ax^p \quad \Rightarrow \quad \log y = p \log x + \log a \tag{4.3}$$

and the resulting coefficients is displayed in plots. The regression is used just as a tool to draw the line over the generated data. This is most noticeable in the three dimensional cases, as shown further on. For the annulus cases, effectively, the first two points are ignored.

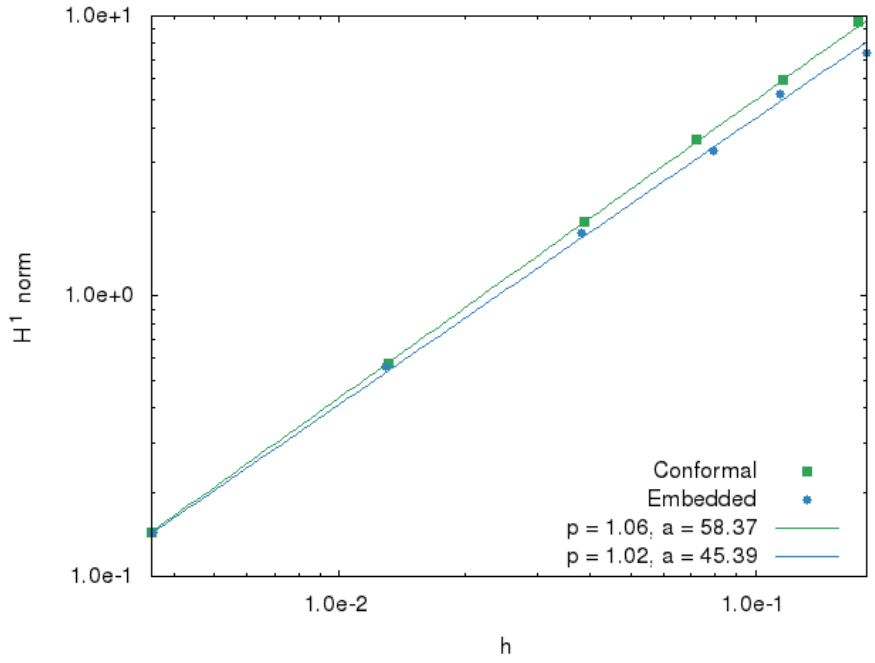

Figure 4.9: H^1 error norms on annular domain.

Table 4.2 shows, for the conformal cases, the evaluated metrics of plot 4.8 and 4.9. The height h_{max} is taken as the maximum of the three heights among all elements, and the ratio A/A_{tot} is a measure of the geometric convergence, being A as the area of the mesh and A_{tot} is the annulus area.

Table 4.2: Evaluated metrics on annulus, conformal formulation.

h_{max}	A/A_{tot}	L^2 norm	H^1 norm
0.175711	0.998139	0.337824	9.59381
0.115835	0.999981	0.112937	5.89528
0.0718044	0.999879	0.0448224	3.62171
0.0388709	0.999989	0.0107932	1.8468
0.0130827	0.999998	0.000999904	0.57555
0.00354168	0.999998	6.17829e-05	0.144027

The same result, now for the Shifted Boundary formulation, is presented in Table 4.3. In this case A is the area of the selected elements to represent the surrogate domain, i.e. the surrogate boundary and the inner elements. By examining the ratio A/A_{tot} one can notice the poor domain representation of the first meshes, nevertheless the presented results shows error distributions similar to its conformal equivalents testifying the robustness of the examined fomulation.

Table 4.3: Evaluated metrics on annulus, shifted boundary formulation.

h_{max}	A/A_{tot}	L^2 norm	H^1 norm
0.0035797	0.557276	1.35667	7.3595
0.184551	0.726799	0.502674	5.26401
0.114021	0.825934	0.197801	3.31077
0.0792705	0.911809	0.0506092	1.67893
0.0382151	0.971010	0.00531394	0.56309
0.0129658	0.992859	0.000358381	0.143651

4.2 Spherical shell evaluation

As for the spherical shell the visualization is not as easy as in the two-dimensional cases, and only the inspection of selected features is possible when not dealing with a virtual model. Besides that, the examined meshes does not get as denser as in the previous examined cases due to the computational limitations of the available resources for this work. Nevertheless the results are satisfactorily in accordance with what is claimed in the formulation proposition.

The resulting field for the five conformal meshes are shown in figure 4.10. The result is presented in a cutted section of the domain. It is possible to notice the decreasing element size as its surface get more spherical as it decreases. The resulting field shows a smooth distribution in accordance with the expected one.

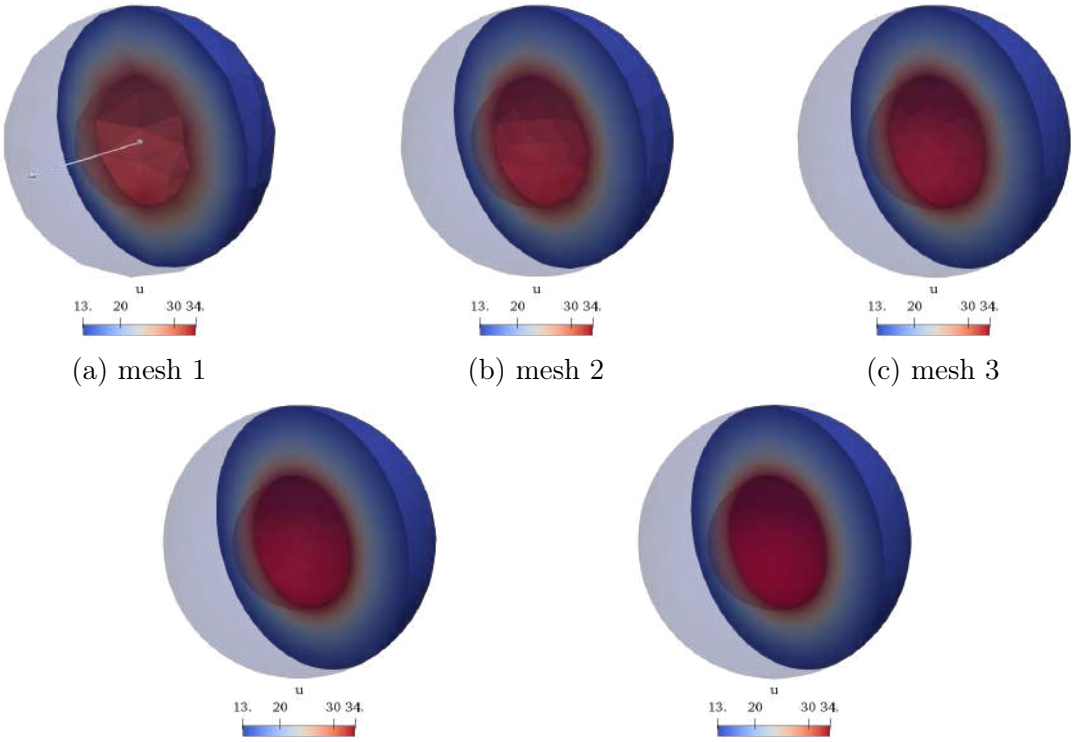

(a) mesh 1 (b) mesh 2 (c) mesh 3

(d) mesh 4 (e) mesh 5

Figure 4.10: Conformal formulation, spherical shell domain.

The equivalent set of results is shown for the shifted boundary formulation in figure 4.11. The displayed volumes are a half volume section of the already filtered surrogate and inner elements. Although in the first two cases, the mesh coarseness is such that it shows no resemblance to the proposed geometry, it is still possible to see the gradient in the expected direction. For the remaining cases the results improves as the mesh gets denser, as expected.

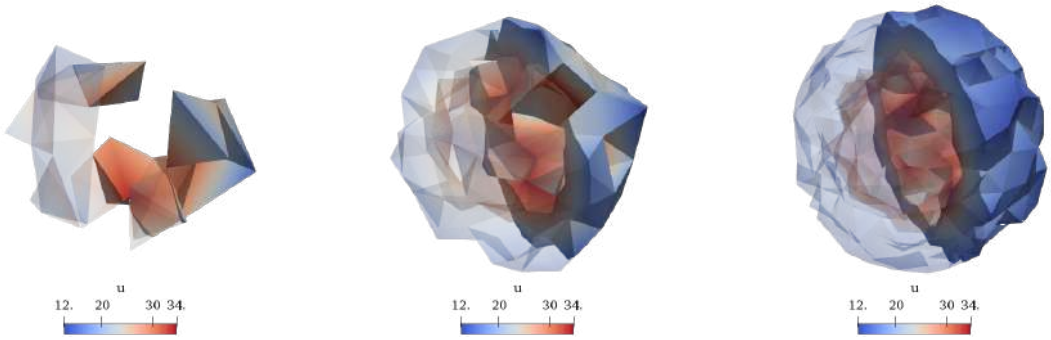

(a) mesh 1 (b) mesh 2 (c) mesh 3

Figure 4.11: Shifted boundary formulation, spherical shell domain (continue).

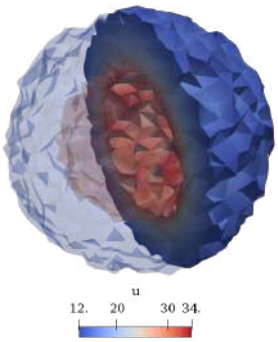

(d) mesh 4

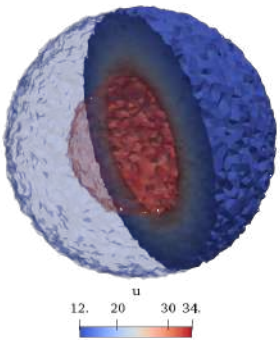

(e) mesh 5

Figure 4.11: Shifted boundary formulation, spherical shell domain.

The analytical solution used as reference for this set of cases is

$$u\left(r(\mathbf{x})\right) = \frac{(u_i T_i - u_e T_e)}{(r_i - r_e)} - \frac{r_i r_e}{r(\mathbf{x})} \frac{(T_i - T_e)}{(r_i - r_e)}, \tag{4.4}$$

where, $r(\mathbf{x}) = (x^2 + y^2 + z^2)^{\frac{1}{2}}$, and its gradient is

$$\nabla u(r(\mathbf{x})) = (T_i - T_e) \frac{r_i r_e}{(r_i - r_e)} \frac{1}{r(\mathbf{x})^3} \begin{Bmatrix} x \\ y \\ z \end{Bmatrix}. \tag{4.5}$$

Besides the error field not being evaluated in these cases, the analytical results are useful for the radial sampling of the resulting scalar field, displayed in figure 4.12. The effect of the coarser meshes on the geometrical convergence can be seen in both formulations, with only the denser meshes displaying a satisfactory result. The spread, at the radius extremes, of the boundary condition values applied to the conformal cases can be seen in figure 4.12a, along with the last three meshes showing a reasonable convergence to the expected solution. For the shifted boundary formulation, the gap between the original boundary and the surrogate one is more pronounced than in the two-dimensional case, and an offset to the expected distribution can be noticed in the coarser meshes. The before mentioned correct gradient direction can be clearly seen, and the convergence to the expected distribution is reached in the denser meshes as well.

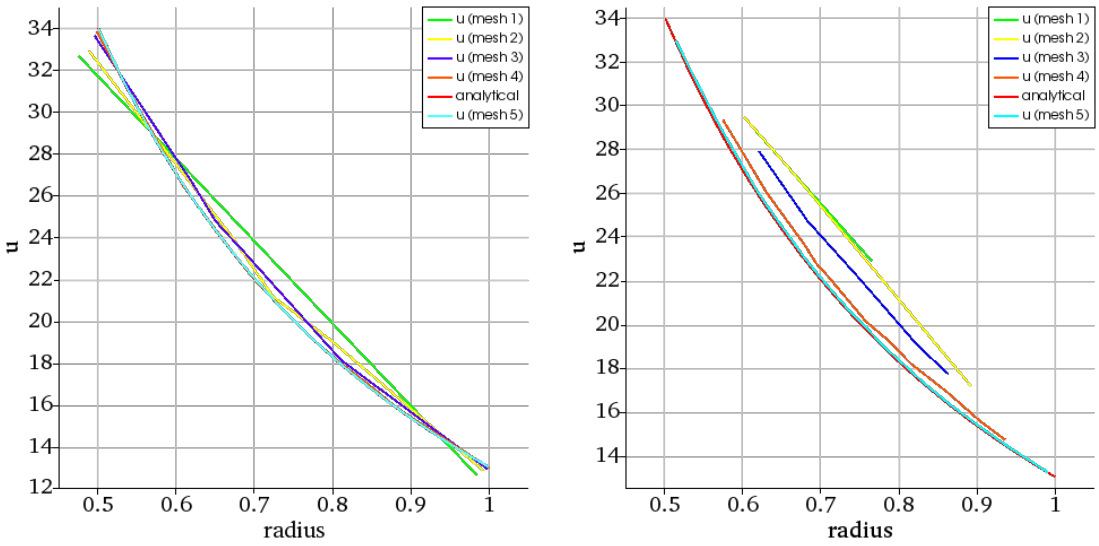

(a) Conformal (b) Shifted boundary

Figure 4.12: Radial sampling of u and u^h on spherical shell domain.

The L^2 error norm evaluation is displayed in figure 4.13, with its resulting coefficients that indicates the expected second order convergence rate, and displaying the same parallel behavior.

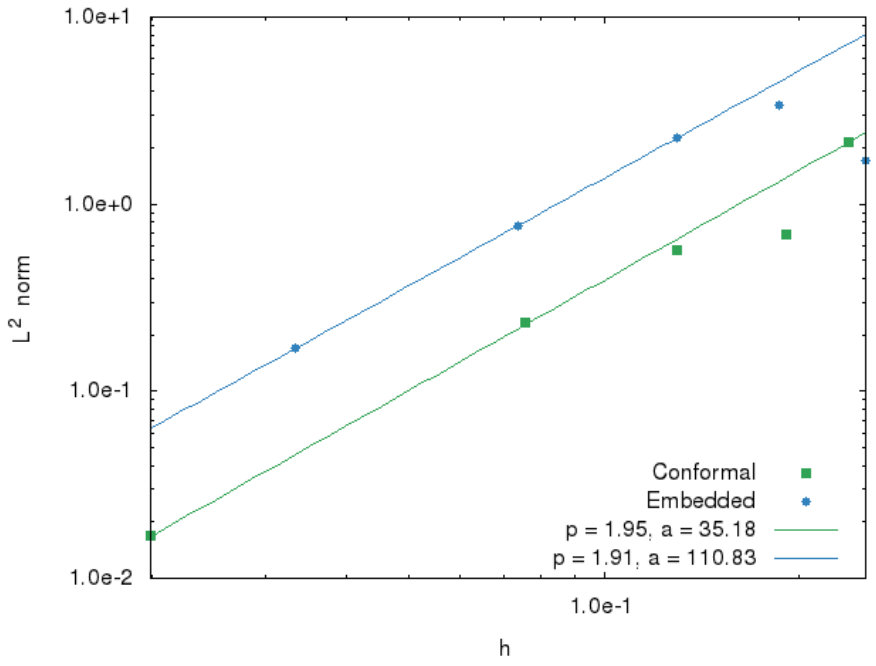

Figure 4.13: L^2 error norms on spherical shell domain.

Due to the poor representation of the coarser meshes, only the three denser ones were selected for the convergence rate evaluation, but all data points are plotted. A linear regression is performed in the same way as before, adjusting variance to craft a tenable convergence line.

The H^1 error norm evaluation is displayed in figure 4.14 and indicates convergence of first order as expected.

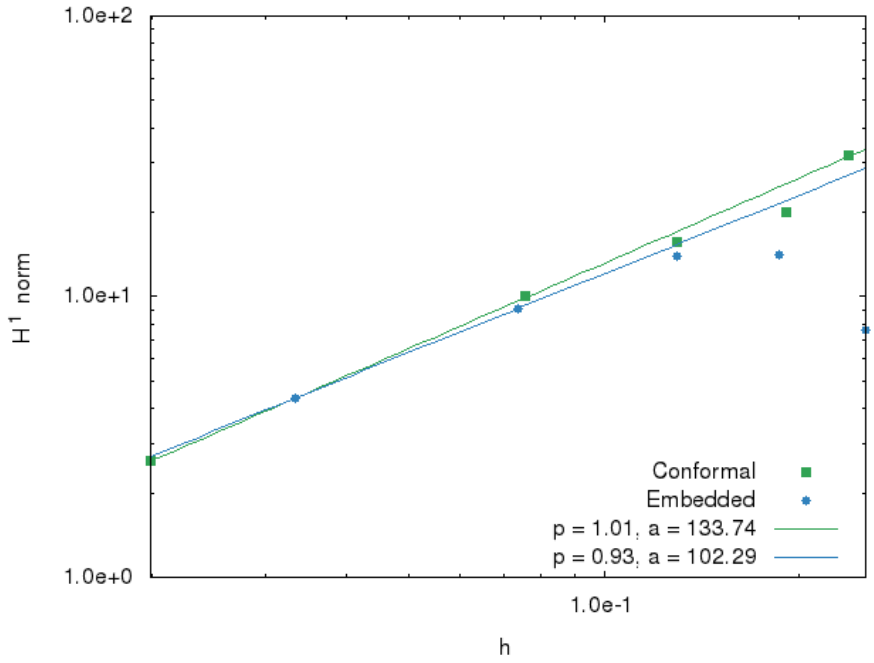

Figure 4.14: H^1 error norms on spherical shell domain.

Table 4.4 shows the same set of evaluated metrics for the conformal formulation, with the geometry convergence being defined as the ratio of the mesh volume and the original geometry volume. The selected results are within the limit of 1% of volume deviation.

Table 4.4: Evaluated metrics on spherical shell, conformal formulation.

h_{max}	V/V_{tot}	L^2 norm	H^1 norm
0.238373	0.972481	2.15471	32.0635
0.1915	0.986101	0.688466	20.103
0.129608	0.994988	0.569275	15.7567
0.0755911	0.998300	0.234023	10.044
0.0199158	0.999893	0.0168134	2.58831

Table 4.5 shows the same metrics for the shifted boundary formulation. The geometry convergence are of an order of magnitude different from the conformal formulation, with the first selected point having a volume deviation superior to 40%. The best result, which is close to indistinguishable from the analytical solution, as shown in 4.12b, has a volume deviation of more than 10%. This result show the robustness of the examined formulation.

Table 4.5: Evaluated metrics on spherical shell, shifted boundary formulation.

h_{max}	V/V_{tot}	L^2 norm	H^1 norm
0.253706	0.085764	1.70056	7.60359
0.186363	0.351510	3.40168	14.1826
0.129608	0.582493	2.25445	14.0146
0.0735193	0.759903	0.76407	9.07175
0.0333763	0.890532	0.171322	4.35821

Chapter 5

Conclusions and Future Works

The conclusions and future works suggestions offers some reflections on the results and the implementation experience, and are considered as valuable as the obtained results. Its main focus is to serve as a stepping stone for the next ones who wishes to venture into the Surrogate Boundary formulation.

5.1 Conclusions

The norm's convergence rate has demonstrated to be quite sensible to how the elements height choice is made. The analytical convergence rate is done aiming to evaluate the minimal necessary element height correspondent to the estimated error. When dealing with a numerical experiment, the used height to fulfill this condition is necessarily the maximum element's maximum height. For the analysis this concept is abstracted out and refereed as the element diameter. A misunderstanding of this condition, conjugated with partitions containing elements with high form factor, in some cases only a few of them, and a wide element's diameter distribution, lead to misleading conclusions during this study and convergence rates close to unreasonable or contrary to what was stated. This difficulty was dealt with by restricting the elements form factor within a deviation of 5% off the characteristic length used by the mesh generator, and the subsequent correct diameter choice.

The final convergence rate was accordant to the reported one, being of second order for the L^2 norm and of first order for the H^1 norm. One can speculate that the discrepancy to the analytical one, in the original work, of order 1.5 for the L^2 norm, might be related to the fact that the residues introduced by the shifted boundary formulation is present only in the surrogate elements and, as the elements diameter diminished, its total area diminishes with an $\mathcal{O}(h^2)$ rate. The relative weight of this area might be an important factor as well, meaning that, for geometries with low $\partial\Gamma/\Omega$ ratio its impact is probably low as well. This supposition is supported by the fact that for the inner elements, both the linear and the bilinear forms are identical

to its equivalent in Nitsche's formulation.

The attempt to implement the formulation along with an adaptive mesh refinement scheme was done, but due to an specific limitation in the framework it was not successful and thus the initially planned scope was reduced. The way libMesh is implemented (version 0.9.4), by adding an element to a mesh, its nodal values are evaluated by interpolating its parent's. When using the subdomains infrastructure the disabled elements don't have its nodal values initialized and thus, when an element is added by including a child of an uninitialized elements a null exception is thrown. The diagnose was done in conjunction with libMesh's support team and by the given answer, it is unlikely that the issue will be addressed in the foreseen future. Nevertheless the idea of adding a geometric convergence criterion to the mesh refinement seems promising.

The formulation might not be directly applicable to cases in which the region close to the boundary is of particular interest or for multi-physics models. A reference surface can be a mean of projecting the computed values onto the original geometry for then properly analyzing them, according to the objective. Before adopting this procedure, it is critical to evaluate its comparable advantage over a classical conformal mesh approach so the introduced complexity does not fall back into an equivalent computational intensive model. This would depend a lot on the nature of the analyzed problem and the adopted implementation strategy.

5.2 Future Works

The implementation of a geometric criterion for an adaptive mesh refinement scheme is manifestly a next step in applying the formulation in real world problem, and it is mostly an implementation problem. For that either a refactoring of the used framework could be done or in a more laborious scope a dedicated implementation can be done starting from scratch. Smarter detection scheme should also be elaborated for geometry varying problems.

The option for representing more complex geometries do not necessarily need to be an unique one, since the geometric evaluations, performed element by element, are embarrassingly parallel and can be interchanged at will. The option of composing geometries by combining elementary analytical shapes with Boolean operation appeals for its simplicity and should be taken as a serious candidate. Other option would be to adopt facet surfaces, being STL surfaces one of the most popular formats. In this case each facet can be used to define an oriented plane and then a ray trace algorithm can be used to evaluate the set of internal nodes. Finally the direct use of any NURBS surface can also be done. In this case the evaluation of the normal and displacement vectors would have to be carefully evaluated so the

computational complexity does not supersede the formulation benefits.

Finally the implementation of more complex physics is an obvious demand. Siblings formulations for Stokes, Navier-Stokes and free-surface problems are already available. For turbulent problems the stability of various Reynolds' number range would have to be judiciously evaluated before adopting the formulation. Another promising application is a fluid-structure interaction problems, where it is possible to couple a flow to structural elements rigidly connected to its geometric surfaces.

Bibliography

[1] BOGGS, P. T., ALTHSULER, A., LARZELERE, A. R., et al. "DART system analysis." doi: 10.2172/876325.

[2] COTTRELL, J. A., HUGHES, T. J., BAZILEVS, Y. *Isogeometric Analysis: Toward Integration of CAD and FEA*. Wiley, 2009. ISBN: 978-0-470-74873-2.

[3] MAIN, A., SCOVAZZI, G. "The shifted boundary method for embedded domain computations. Part I: Poisson and Stokes problems", *Journal of Computational Physics*, v. 372, pp. 972 – 995, 2018. ISSN: 0021-9991. doi: https://doi.org/10.1016/j.jcp.2017.10.026. Disponível em: <http://www.sciencedirect.com/science/article/pii/S0021999117307799>.

[4] MAIN, A., SCOVAZZI, G. "The shifted boundary method for embedded domain computations. Part II: Linear advection–diffusion and incompressible Navier–Stokes equations", *Journal of Computational Physics*, v. 372, pp. 996 – 1026, 2018. ISSN: 0021-9991. doi: https://doi.org/10.1016/j.jcp.2018.01.023. Disponível em: <http://www.sciencedirect.com/science/article/pii/S0021999118300330>.

[5] PESKIN, C. S. "Flow patterns around heart valves: A numerical method", *Journal of Computational Physics*, v. 10, n. 2, pp. 252 – 271, 1972. ISSN: 0021-9991. doi: http://dx.doi.org/10.1016/0021-9991(72)90065-4. Disponível em: <http://www.sciencedirect.com/science/article/pii/0021999172900654>.

[6] DUNNE, T. "An Eulerian approach to fluid–structure interaction and goal-oriented mesh adaptation", *International Journal for Numerical Methods in Fluids*, v. 51, n. 9-10, pp. 1017–1039, 2006. doi: 10.1002/fld.1205. Disponível em: <https://onlinelibrary.wiley.com/doi/abs/10.1002/fld.1205>.

[7] MOËS, N., DOLBOW, J., BELYTSCHKO, T. "A finite element method for crack growth without remeshing", *International*

Journal for Numerical Methods in Engineering, v. 46, n. 1, pp. 131–150. doi: 10.1002/(SICI)1097-0207(19990910)46:1<131::AID-NME726>3.0.CO;2-J. Disponível em: <https://onlinelibrary.wiley.com/doi/abs/10.1002/%28SICI%291097-0207%2819990910%2946%3A1%3C131%3A%3AAID-NME726%3E3.0.CO%3B2-J>.

[8] NITSCHE, J. "Über ein Variationsprinzip zur Lösung von Dirichlet-Problemen bei Verwendung von Teilräumen, die keinen Randbedingungen unterworfen sind", *Abhandlungen aus dem Mathematischen Seminar der Universität Hamburg*, v. 36, n. 1, pp. 9–15, 1971. ISSN: 1865-8784. doi: 10.1007/BF02995904. Disponível em: <http://dx.doi.org/10.1007/BF02995904>.

[9] HANSBO, A., HANSBO, P. "An unfitted finite element method, based on Nitsche's method, for elliptic interface problems", *Computer Methods in Applied Mechanics and Engineering*, v. 191, n. 47, pp. 5537 – 5552, 2002. ISSN: 0045-7825. doi: https://doi.org/10.1016/S0045-7825(02)00524-8. Disponível em: <http://www.sciencedirect.com/science/article/pii/S0045782502005248>.

[10] SCHILLINGER, D., DÜSTER, A., RANK, E. "The hp-d-adaptive finite cell method for geometrically nonlinear problems of solid mechanics", *International Journal for Numerical Methods in Engineering*, v. 89, n. 9, pp. 1171–1202, 2012. ISSN: 1097-0207. doi: 10.1002/nme.3289. Disponível em: <http://dx.doi.org/10.1002/nme.3289>.

[11] XU, F., SCHILLINGER, D., KAMENSKY, D., et al. "The tetrahedral finite cell method for fluids: Immersogeometric analysis of turbulent flow around complex geometries", *Computers & Fluids*, v. 141, pp. 135 – 154, 2016. ISSN: 0045-7930. doi: http://dx.doi.org/10.1016/j.compfluid.2015.08.027. Disponível em: <http://www.sciencedirect.com/science/article/pii/S0045793015003035>. Advances in Fluid-Structure Interaction.

[12] SCHILLINGER, D., RUESS, M. "The Finite Cell Method: A Review in the Context of Higher-Order Structural Analysis of CAD and Image-Based Geometric Models", *Archives of Computational Methods in Engineering*, v. 22, n. 3, pp. 391–455, Jul 2015. ISSN: 1886-1784. doi: 10.1007/s11831-014-9115-y. Disponível em: <https://doi.org/10.1007/s11831-014-9115-y>.

[13] KIRK, B. S., PETERSON, J. W., STOGNER, R. H., et al. "libMesh : a C++ library for parallel adaptive mesh refinement/coarsening simula-

tions", *Engineering with Computers*, v. 22, n. 3, pp. 237–254, 2006. ISSN: 1435-5663. doi: 10.1007/s00366-006-0049-3. Disponível em: <http://dx.doi.org/10.1007/s00366-006-0049-3>.

[14] FREUND, J., STENBERG, R. "On weakly imposed boundary conditions for second order problems", *Proceedings of the Ninth International Conference on Finite Elements in Fluids*, pp. 327–336, 01 1995.

[15] HADAMARD, J. "Théorie des équations aux dérivées partielles linéaires hyperboliques et du problème de Cauchy", *Acta Math.*, v. 31, pp. 333–380, 1908. doi: 10.1007/BF02415449. Disponível em: <https://doi.org/10.1007/BF02415449>.

[16] ALEXANDRE ERN, J.-L. G. Springer, 2004. ISBN: 0387205748. Disponível em: <https://www.springer.com/gp/book/9780387205748/>.

[17] "libMesh Official Page". Disponível em: <https://libmesh.github.io/>.

[18] DOUGLAS, J., DUPONT, T. "Interior Penalty Procedures for Elliptic and Parabolic Galerkin Methods". In: Glowinski, R., Lions, J. L. (Eds.), *Computing Methods in Applied Sciences*, pp. 207–216, Berlin, Heidelberg, 1976. Springer Berlin Heidelberg. ISBN: 978-3-540-37550-0.

Appendix A

Definitions

The following definitions and equations are common tools used in the functional analysis and topology fields. It by no means intend to be a systematic presentation of the field, but a starting point for those not familiarized with them.

A.1 Inner Product properties

The inner product is a generalization of the dot product, a bilinear function defined in a Cartesian space. Its operator notation is usually assumed as $\langle \cdot, \cdot \rangle$. The four properties that defines an inner product are known as the positive-definite condition and they are,

1. $\langle u + v, w \rangle = \langle u, w \rangle + \langle v, w \rangle$
2. $\langle \alpha v, w \rangle = \alpha \langle v, w \rangle$
3. $\langle v, w \rangle = \langle w, v \rangle$
4. $\langle v, v \rangle \geq 0$ *and equals only if* $v = 0$

A.2 Norm properties

A norm is a real valued function which has the following properties:

1. Every vector has positive norm, and only the $\mathbf{0}$ vector has zero norm,
   $\| \mathbf{x} \| \geq 0$ and $\| \mathbf{x} \| = 0 \iff \mathbf{x} = \mathbf{0}, \forall \mathbf{x} \in W$
2. Scalar multiplication,
   $\| \alpha \mathbf{x} \| = |\alpha| \, \| \mathbf{x} \|$, $\forall \alpha \in \mathbb{R}$, $\forall \mathbf{x} \in W$
3. Triangle inequality,
   $\| \mathbf{x} + \mathbf{y} \| \leq \| \mathbf{x} \| + \| \mathbf{y} \|$.

Whenever an inner product, using the same element as parameters, also fulfills these properties, i.e. $\langle u, u\rangle = \| \mathbf{x} \|^2$, its is said that the norm is induced by the inner product. In this case the spaces is both a Banach (a normed space) and a Hilbert space (an inner product space). For Hilbert spaces the well posedness of a problem can be assured by means of the the Lax-Milgram theorem and for the Banach space the Banach-Nečas-Babuška theorem [16].

A.3 Spaces and Norms Definitions

The Sobolev space is defined by

$$W_P^s(\Omega) = \left\{ f \in L^P(\Omega); \forall |\alpha| < s, \partial_x^\alpha f \in L^P(\Omega) \right\}, \tag{A.1}$$

where Ω is an open set of $\mathbb{R}_d$, $\alpha = (\alpha_1, \ldots, \alpha_d)$, $|\alpha| = \alpha_1 + \ldots + \alpha_p$, and the operator $\partial_x^\alpha f = (\partial_{x_1}^{\alpha_1}, \ldots, \partial_{x_P}^{\alpha_P})$, with $\{\alpha_i, s\} \in N$ and $d \in N^*$.

The norm for such space is defined starting from the p-norm, of an L^p space:

$$\| f \|_{W_P^s(\Omega)} = \sum_{|\alpha| \leq s} \| \partial_x^\alpha f \|_{L^P(\Omega)} . \tag{A.2}$$

So the space of square integrable functions $L^2(\Omega)$ can be expressed as $L^2(\Omega) = W_s^0(\Omega)$ and its norm $\| f \|_{L^2,\Omega} = \| f \|_{0,\Omega}$. The benefit of operating functions in this space is that the second order p-norm is induced by the inner product and so it is also a Hilbert space.

A.4 Young Inequality

$$ab \leq \frac{1}{2}\left(a^2 + b^2\right), \qquad a, b \in \mathbb{R} \tag{A.3}$$

A.5 Epsilon Inequality

The ϵ-inequality can be promptly derived from Young's inequality as follows

$$\left(\epsilon^{\frac{1}{2}} a\right)\left(\epsilon^{-\frac{1}{2}} b\right) \leq \frac{1}{2}\left[\left(\epsilon^{\frac{1}{2}} a\right)^2 + \left(\epsilon^{-\frac{1}{2}} b\right)^2\right], \tag{A.4}$$

giving for $a, b \in \mathbb{R}$,

$$ab \leq \frac{1}{2}\left(\epsilon a^2 + \frac{b^2}{\epsilon}\right), \qquad \forall \epsilon \in \mathbb{R}_+. \tag{A.5}$$

A.6 Cauchy-Schwartz Inequality

Given $v, w \in V$, where V is a vector space equipped with an inner product $(\cdot, \cdot)$ and norm $\| v \| = (v, v)^{\frac{1}{2}}$, the inequality

$$(v, w)^2 \leq (v, v)\,(w, w) \Rightarrow (v, w) \leq |\,(v, w)\,| \leq \| v \| \| w \| \tag{A.6}$$

holds true and is refereed as Cauchy-Schwartz inequality.

Since the right most terms are scalars, it is possible, by using the ϵ-inequality, to compose the following inequality

$$(v, w) \leq \frac{1}{2}\left(\epsilon \| v \|^2 + \frac{\| w \|^2}{\epsilon}\right) \tag{A.7}$$

that is used in the coercivity evaluation.

A.7 Discrete Trace Inequality

The discrete trace inequality is proven by Douglas [18] and is stated here, in its reduced version, for piecewise linear and globally continuous functions, as a lemma:

$$\| \left(h^{\perp}\right)^{\frac{1}{2}} \nabla w \cdot \mathbf{v} \|^2_{0,\Gamma} \leq C_I \| \nabla w \|^2_{0,\Omega}\,. \tag{A.8}$$

where $h^{\perp}$ is the element height as defined before, and $C_I \in \mathbb{R}^*_+$. The inequality

$$\| \left(h^{\perp}\right)^{\frac{1}{2}} \nabla w \cdot \mathbf{v} \|_{0,\Gamma} \leq C_I \| \nabla w \|_{0,\Omega} \tag{A.9}$$

is a corollary and is the one used in the continuity evaluation.

A.8 Auxiliary Inequality

Given six non-negative scalars $a, b, c, d, e, f \in \mathbb{R}^+$, the inequality

$$ad + ae + db + be \leq \left(a^2 + b^2 + c^2\right)\left(d^2 + e^2 + f^2\right), \tag{A.10}$$

is true and is stated for clarity, as it is used as argument for the continuity demonstration.

Appendix B

Bilinear Form Analysis

The well-posednes of the problem is assured provided the Lax-Milgram theorem's conditions are verified [16], meaning the bilinear form needs to be coercive and continuous, as well as consistent. These properties are proved in the original work [3] and are here after examined.

B.1 Coercivity

Taking the bilinear form stated in equation 2.18 and applying u^h in both arguments:

$$\begin{aligned} a\left(u^h,u^h\right) = &\left(\nabla u^h,\nabla u^h\right)_{\widetilde{\Omega}} \\ &-\langle u^h+\nabla u^h\cdot\mathbf{d},\nabla u^h\cdot\widetilde{\mathbf{n}}\rangle_{\widetilde{\Gamma}_D}-\langle\nabla u^h\cdot\widetilde{\mathbf{n}},u^h+\nabla u^h\cdot\mathbf{d}\rangle_{\widetilde{\Gamma}_D} \\ &+\langle\nabla u^h\cdot\mathbf{d},\frac{\mathbf{n}\cdot\widetilde{\mathbf{n}}}{\parallel\mathbf{d}\parallel}\nabla u^h\cdot\mathbf{d}\rangle_{\widetilde{\Gamma}_D}+\eta\langle u^h+\nabla u^h\cdot\mathbf{d},u^h+\nabla u^h\cdot\mathbf{d}\rangle_{\widetilde{\Gamma}_D}. \end{aligned} \tag{B.1}$$

Using the norms defined in section A.3:

$$\begin{aligned} a\left(u^h,u^h\right) = &\parallel\nabla u^h\parallel^2_{0,\widetilde{\Omega}}-2\langle u^h+\nabla u^h\cdot\mathbf{d},\nabla u^h\cdot\widetilde{\mathbf{n}}\rangle_{\widetilde{\Gamma}_D} \\ &+\parallel\left(\frac{\mathbf{n}\cdot\widetilde{\mathbf{n}}}{\parallel\mathbf{d}\parallel}\right)^{\frac{1}{2}}\nabla u^h\cdot\mathbf{d}\parallel^2_{0,\widetilde{\Gamma}_D}+\alpha h^{\perp^{-1}}\parallel u^h+\nabla u^h\cdot\mathbf{d}\parallel^2_{0,\widetilde{\Gamma}_D}. \end{aligned} \tag{B.2}$$

Taking the second term of the left hand side of previous equation and applying the ϵ-inequality and Cauchy-Schwartz, as stated in equation A.7, gives

$$2\langle u^h+\nabla u^h\cdot\mathbf{d},\nabla u^h\cdot\widetilde{\mathbf{n}}\rangle_{\widetilde{\Gamma}_D}\leq\left(\epsilon h^{\perp}\right)^{-1}\parallel u^h+\nabla u^h\cdot\mathbf{d}\parallel^2_{0,\widetilde{\Gamma}_D}+\epsilon h^{\perp}\parallel\nabla u^h\cdot\mathbf{d}\parallel^2_{0,\widetilde{\Gamma}_D}. \tag{B.3}$$

By substituting equation B.3 in B.2 gives

$$\begin{aligned} a\left(u^h,u^h\right)\geq &\parallel\nabla u^h\parallel^2_{0,\widetilde{\Omega}}+\left(\alpha-\epsilon^{-1}\right)h^{\perp^{-1}}\parallel u^h+\nabla u^h\cdot\mathbf{d}\parallel^2_{0,\widetilde{\Gamma}_D} \\ &-\epsilon h^{\perp}\parallel\nabla u^h\cdot\widetilde{\mathbf{n}}\parallel^2_{0,\widetilde{\Gamma}_D}+\parallel\left(\frac{\mathbf{n}\cdot\widetilde{\mathbf{n}}}{\parallel\mathbf{d}\parallel}\right)^{\frac{1}{2}}\nabla u^h\cdot\mathbf{d}\parallel^2_{0,\widetilde{\Gamma}_D}. \end{aligned} \tag{B.4}$$

By using inequality A.8 on the third term of the right hand side we have,

$$-\epsilon h^{\perp} \parallel \nabla u^h \cdot \widetilde{\mathbf{n}} \parallel^2_{0,\widetilde{\Gamma}_D} \geq -\epsilon C_I \parallel \nabla u^h \parallel^2_{0,\widetilde{\Omega}}, \tag{B.5}$$

that finally gives

$$\begin{aligned} a\left(u^h, u^h\right) \geq & (1-\epsilon C_I) \parallel \nabla u^h \parallel^2_{0,\widetilde{\Omega}} \\ & + \left(\alpha - \epsilon^{-1}\right) h^{\perp -1} \parallel u^h + \nabla u^h \cdot \mathbf{d} \parallel^2_{0,\widetilde{\Gamma}_D} \\ & + \parallel \left(\frac{\mathbf{n}\cdot\widetilde{\mathbf{n}}}{\parallel \mathbf{d} \parallel}\right)^{\frac{1}{2}} \nabla u^h \cdot \mathbf{d} \parallel^2_{0,\widetilde{\Gamma}_D} \geq 0, \end{aligned} \tag{B.6}$$

that is true, since, by definition, every norm is greater or equal to zero, being $h^{\perp}$ a positive number; ϵ is arbitrarily small and also positive, as restricted by inequality A.4; C_I is positive, as assumed by inequality A.8. This leads to the inequalities

$$\begin{aligned} (1-\epsilon C_I) > 0 \quad &\Longleftrightarrow \quad \epsilon < \frac{1}{C_I} \\ \left(\alpha - \frac{1}{\epsilon}\right) > 0 \quad &\Longleftrightarrow \quad \alpha > \frac{1}{\epsilon} \end{aligned} \tag{B.7}$$

also being held true. This way, by defining a norm $\parallel \cdot \parallel^2_{SB}$ as,

$$\begin{aligned} \parallel u^h \parallel^2_{SB} = & \parallel \nabla u^h \parallel^2_{0,\widetilde{\Omega}} + \frac{1}{h^{\perp}} \parallel u^h + \nabla u^h \cdot \mathbf{d} \parallel^2_{0,\widetilde{\Gamma}} \\ & + \frac{\mathbf{n}\cdot\widetilde{\mathbf{n}}}{\mathbf{d}} \parallel \nabla u^h \cdot \mathbf{n} \parallel^2_{0,\widetilde{\Gamma}}, \end{aligned} \tag{B.8}$$

the stability is proven by the coercivity argument, since

$$a^h\left(u^h, u^h\right) \geq C_{SB} \parallel u^h \parallel^2_{SB} z \tag{B.9}$$

provided

$$C_{SB} = min\left\{1-\epsilon C_I, \alpha - \frac{1}{\epsilon}\right\}. \tag{B.10}$$

B.2 Continuity

The continuity is demonstrated by taking the norm defined in B.8 and demonstrating that, for the bilinear form stated in 2.18, the inequality

$$a^h\left(u^h, v^h\right) \leq C_b \parallel u^h \parallel_{SB} \parallel v^h \parallel_{SB} \tag{B.11}$$

is true. The inequality is demonstrated by numbering the terms as

$$
\begin{aligned}
a^h\left(u^h, v^h\right) = & \left(\nabla v^h, \nabla u^h\right)_{\widetilde{\Omega}} && (1)\\
& - \left\langle v^h + \nabla v^h \cdot \mathbf{d}, \nabla u^h \cdot \widetilde{\mathbf{n}} \right\rangle_{\tilde{\Gamma}_D} && (2)\\
& - \left\langle \nabla v^h \cdot \widetilde{\mathbf{n}}, u^h + \nabla u^h \cdot \mathbf{d} \right\rangle_{\tilde{\Gamma}_D} && (3)\\
& + \left\langle \nabla v^h \cdot \mathbf{d}, \frac{(\mathbf{n} \cdot \tilde{\mathbf{n}})}{\|\mathbf{d}\|} \nabla u^h \cdot \mathbf{d} \right\rangle_{\tilde{\Gamma}_D} && (4)\\
& + \frac{\alpha}{h^\perp} \left\langle v^h + \nabla v^h \cdot \mathbf{d}, u^h + \nabla u^h \cdot \mathbf{d} \right\rangle_{\tilde{\Gamma}_D} && (5)
\end{aligned}
$$

and reasoning about them separately. The norms presented in A.3 are used and can be recognized by adopted nomenclature.

For the first term, by taking inequality A.6 give

$$
\left(\nabla v^h, \nabla u^h\right) \leq \| \nabla v^h \|_{0,\widetilde{\Omega}} \| \nabla u^h \|_{0,\widetilde{\Omega}} . \tag{B.12}
$$

The second term also takes the inequality A.6 giving

$$
\left\langle v^h + \nabla v^h \cdot \mathbf{d}, \nabla u^h \cdot \widetilde{\mathbf{n}} \right\rangle_{\tilde{\Gamma}_D} \leq \left|\left| \sqrt{\frac{1}{h^\perp}} \left(v^h + \nabla v^h \cdot \mathbf{d}\right) \right|\right|_{0,\widetilde{\Gamma}} \left|\left| \sqrt{h^\perp} \nabla u^h \cdot \mathbf{n} \right|\right|_{0,\widetilde{\Gamma}}, \tag{B.13}
$$

where the terms containing $h^\perp$ are introduced so the inequality A.9 can then be applied giving

$$
\left\langle v^h + \nabla v^h \cdot \mathbf{d}, \nabla u^h \cdot \widetilde{\mathbf{n}} \right\rangle_{\tilde{\Gamma}_D} \leq \left|\left| \sqrt{\frac{1}{h^\perp}} \left(v^h + \nabla v^h \cdot \mathbf{d}\right) \right|\right|_{0,\widetilde{\Gamma}} C_I \left|\left| \nabla u^h \right|\right|_{0,\widetilde{\Omega}} . \tag{B.14}
$$

The same procedure is applied to the third term which then gives

$$
\left\langle \nabla v^h \cdot \widetilde{\mathbf{n}}, u^h + \nabla u^h \cdot \mathbf{d} \right\rangle_{\tilde{\Gamma}_D} \leq C_I \left|\left| \nabla v^h \right|\right|_{0,\widetilde{\Omega}} \left|\left| \sqrt{\frac{1}{h^\perp}} \left(u^h + \nabla u^h \cdot \mathbf{d}\right) \right|\right|_{0,\widetilde{\Gamma}} . \tag{B.15}
$$

As for the fourth term, by assuming $0 \leq \mathbf{n} \cdot \widetilde{\mathbf{n}} \leq 1$, necessary condition for inequality A.8, also that $\|\mathbf{d}\|/h^\perp \leq 1$, since it is reasonable to assume the distance will never be greater than the maximum element height, and finally that $\mathbf{n} = \mathbf{d}/\|\mathbf{d}\|$, meaning the displacement vector is aligned with the original boundary norm, we can state that

$$
\left\langle \nabla v^h \cdot \mathbf{d}, \frac{(\mathbf{n} \cdot \tilde{\mathbf{n}})}{\|\mathbf{d}\|} \nabla u^h \cdot \mathbf{d} \right\rangle_{\tilde{\Gamma}_D} \leq \left\langle \frac{h^\perp}{\|\mathbf{d}\|} \nabla v^h \cdot \mathbf{d}, \nabla u^h \cdot \mathbf{n} \right\rangle_{\tilde{\Gamma}_D}, \tag{B.16}
$$

which leads to

$$
\left\langle \nabla v^h \cdot \mathbf{d}, \frac{(\mathbf{n} \cdot \tilde{\mathbf{n}})}{\|\mathbf{d}\|} \nabla u^h \cdot \mathbf{d} \right\rangle_{\tilde{\Gamma}_D} \leq \left\langle \sqrt{h^\perp} \nabla v^h \cdot \mathbf{n}, \sqrt{h^\perp} \nabla u^h \cdot \mathbf{n} \right\rangle_{\tilde{\Gamma}_D}, \tag{B.17}
$$

and finally, by using inequality A.9 gives

$$\left\langle \nabla v^h \cdot \mathbf{d}, \frac{(\mathbf{n}\cdot\tilde{\mathbf{n}})}{\|\mathbf{d}\|}\nabla u^h \cdot \mathbf{d} \right\rangle_{\tilde{\Gamma}_D} \leq C_I^2 \|\nabla v^h\|_{0,\widetilde{\Omega}} \|\nabla u^h\|_{0,\widetilde{\Omega}}. \tag{B.18}$$

As for the last terms assuming a similar procedure, as in the second and third term, gives

$$\begin{aligned} &\alpha \left\langle \sqrt{\frac{1}{h^\perp}} \left(v^h + \nabla v^h \cdot \mathbf{d}\right), \sqrt{\frac{1}{h^\perp}} \left(u^h + \nabla u^h \cdot \mathbf{d}\right) \right\rangle_{\tilde{\Gamma}_D} \\ \leq \alpha &\left\| \sqrt{\frac{1}{h^\perp}} v^h + \nabla v^h \cdot \mathbf{d} \right\|_{0,\widetilde{\Gamma}_D} \left\| \sqrt{\frac{1}{h^\perp}} u^h + \nabla u^h \cdot \mathbf{d} \right\|_{0,\widetilde{\Gamma}_D}. \end{aligned} \tag{B.19}$$

Since all five terms have a positive upper boundary, it is possible to invert the sign of the second and third term, giving the inequality

$$\begin{aligned} a^h\left(u^h, v^h\right) \leq &\parallel \nabla v^h \parallel_{0,\widetilde{\Omega}} \parallel \nabla u^h \parallel_{0,\widetilde{\Omega}} \\ &+ \left\| \sqrt{\frac{1}{h^\perp}} \left(v^h + \nabla v^h \cdot \mathbf{d}\right) \right\|_{0,\widetilde{\Gamma}} C_I \left|\left|\nabla u^h\right|\right|_{0,\widetilde{\Omega}} \\ &+ C_I \left|\left|\nabla v^h\right|\right|_{0,\widetilde{\Omega}} \left\| \sqrt{\frac{1}{h^\perp}} \left(u^h + \nabla u^h \cdot \mathbf{d}\right) \right\|_{0,\widetilde{\Gamma}} \\ &+ C_I^2 \|\nabla v^h\|_{0,\widetilde{\Omega}} \|\nabla u^h\|_{0,\widetilde{\Omega}} \\ &+ \alpha \left\| \sqrt{\frac{1}{h^\perp}} v^h + \nabla v^h \cdot \mathbf{d} \right\|_{0,\widetilde{\Gamma}_D} \left\| \sqrt{\frac{1}{h^\perp}} u^h + \nabla u^h \cdot \mathbf{d} \right\|_{0,\widetilde{\Gamma}_D} \\ \leq &C_b \parallel u^h \parallel_{SB} \parallel v^h \parallel_{SB}. \end{aligned} \tag{B.20}$$

The right most inequality is placed by mean of argument placed in inequality A.10, finally proving B.11, provided $C_b = max\left\{1 + C_I^2, \alpha\right\}$.

B.3 Consistency

Whenever the exact solution of a model is applied to an equivalent variational formulation, the formulation is said to be consistent when its resulting residue is zero, i.e. for a generic problem defined by $a(u^h, v^h)$ and $l(v^h)$ with an exact solution u, we have

$$a^h(u, v^h) - l(v^h) = 0. \tag{B.21}$$

This mean the error of the projected solution is perpendicular to the space in which the formulation is defined.

For the surrogate boundary, since the domain varies with the adopted space partition and is supposed not to match the original one, the consistency is assumed

to be asymptotic, i.e. it is as small as the partition diameter but never zero, in other words, for a generic asymptotic formulation applied to a surrogate domain $\widetilde{\Omega}$ we have

$$\widetilde{a}^h(u, v^h) - \widetilde{l}^h(v) = O(h^k). \tag{B.22}$$

This applied to the examined formulation then give,

$$\begin{aligned}\widetilde{a}^h(u, v^h) - \widetilde{l}^h(v) =& (\nabla v^h, \nabla u)_{\widetilde{\Omega}} - \left\langle v^h, \nabla u \cdot \widetilde{\mathbf{n}} \right\rangle_{\widetilde{\Gamma}_D} - (v^h, f)_{\widetilde{\Omega}} \\ &- \left\langle \nabla v^h \cdot \mathbf{d}, \nabla u \cdot \widetilde{\mathbf{n}} \right\rangle_{\widetilde{\Gamma}_D} \\ &- \left\langle \nabla v^h \cdot \widetilde{\mathbf{n}}, u + \nabla u \cdot \mathbf{d} - \overline{u}_D \right\rangle_{\widetilde{\Gamma}_D} \\ &+ \left\langle \frac{\alpha}{h^\perp}(v^h + \nabla v^h \cdot \mathbf{d}), u + \nabla u \cdot \mathbf{d} - \overline{u}_D \right\rangle_{\widetilde{\Gamma}_D} \\ &+ \left\langle \nabla v^h \cdot \mathbf{d}, (\mathbf{n} \cdot \widetilde{\mathbf{n}}) \nabla u \cdot \mathbf{n} + (\tau_i \cdot \widetilde{\mathbf{n}}) \nabla u \cdot \tau_i \right\rangle_{\widetilde{\Gamma}_D},\end{aligned} \tag{B.23}$$

which by considering the fact that the right hand side on the first line is equivalent to the classical formulation, so it is consistent, and also that $u|_{\Gamma_D} = \overline{u}_D$ and that $\nabla u \cdot \mathbf{d}$ is a second order term, we can state that

$$\widetilde{a}^h(u, v^h) - \widetilde{l}^h(v) \leq \| v^h \|_{SB} \, O(h^2), \tag{B.24}$$

leading to the conclusion the formulation is asymptotic consistent.

Appendix C

Analytical Solutions

Both examined cases are an homogeneous diffusive problem

$$\nabla^2\phi(\mathbf{x}) = 0 \tag{C.1}$$

and for the proposed geometries, annulus and spherical shell, they are easier managed on polar and spherical coordinates. The solution for a constant Dirichlet boundary condition is shown bellow.

C.1 Annulus

The diffusive equation in polar coordinates is written as

$$\nabla\phi(r,\theta) = \frac{1}{r}\frac{\partial}{\partial r}\left(r\frac{\partial\phi}{\partial r}\right) + \frac{1}{r^2}\frac{\partial^2\phi}{\partial\theta^2} = 0. \tag{C.2}$$

The boundary condition that defines the problem is

$$\phi(r_i,\theta) = \phi_i \quad \text{and} \quad \phi(r_e,\theta) = \phi_e \tag{C.3}$$

where r_i and r_e are the inner and outer radius, respectively.

By using the separation of variables method one can assume

$$\phi(r,\theta) = R(r)T(\theta), \tag{C.4}$$

which gives, by substituting it in equation C.2,

$$\frac{r}{R}\left(r\frac{dR}{dr}\right) + \frac{1}{T}\frac{d^2}{d\theta^2} = 0. \tag{C.5}$$

Since, for the given boundary condition, the resulting scalar field has radial symmetry, the second term is null leading to an ordinary equation, which after integrating gives

$$\phi(r) = A_0 + B_0 \ln r. \tag{C.6}$$

By using the boundary condition we have

$$A_0 = \phi_i - \frac{(\phi_e - \phi_i)}{\ln\left(\frac{r_e}{r_i}\right)} \ln r_i \quad \text{and} \quad B_0 = \frac{(\phi_e - \phi_i)}{\ln\left(\frac{r_e}{r_i}\right)}, \tag{C.7}$$

which then results in the final solution

$$\phi(r) = (\phi_e - \phi_i)\frac{\ln {}^{r}/_{r_i}}{\ln {}^{r_e}/_{r_i}} + \phi_i. \tag{C.8}$$

C.2 Spherical Shell

The diffusive equation in spherical coordinate is written as

$$\nabla^2\phi(r,\theta,\varphi) = \frac{1}{r^2}\frac{\partial}{\partial r^2}\left(r\frac{\partial^2\phi}{\partial r^2}\right) + \frac{1}{r^2 sin\theta}\frac{\partial}{\partial\theta}\left(sin\theta\frac{\partial\phi}{\partial\theta}\right) + \frac{1}{r^2 sin^2\theta}\frac{\partial^2\phi}{\partial\varphi^2} = 0. \tag{C.9}$$

The boundary conditions are

$$\phi(r_i,\theta,\varphi) = \phi_i \quad \text{and} \quad \phi(r_e,\theta,\varphi) = \phi_e \tag{C.10}$$

where r_i and r_e are the inner and outer radius, as defined before.

By using the separation of variables method we can assume

$$\phi(r,\theta,\varphi) = R(r)Y(\theta,\varphi) \tag{C.11}$$

which gives, by substituting it in equation C.9,

$$\frac{1}{R}\frac{d}{dr}\left(r^2\frac{dR}{dr}\right) + \frac{1}{Y sin\theta}\frac{\partial}{\partial\theta}\left(sin\theta\frac{\partial Y}{\partial\theta}\right) + \frac{1}{Y sin^2\theta}\frac{\partial^2\phi}{\partial\varphi^2} = 0. \tag{C.12}$$

As before the problem also has radial symmetry, leading to an ordinary differential equation resulting in

$$\phi(r) = A_0 + \frac{B_0}{r}, \tag{C.13}$$

which by utilizing the boundary condition gives

$$A_0 = \frac{\phi_e r_e - \phi_i r_i}{r_e - r_i} \quad \text{and} \quad B_0 = r_i r_e \frac{\phi_e - \phi_i}{r_e - r_i}, \tag{C.14}$$

which leads the final equation

$$\phi(r) = \left(\frac{\phi_e r_e - \phi_i r_i}{r_e - r_i}\right) - \left(\frac{\phi_e - \phi_i}{r_e - r_i}\right)\frac{r_i r_e}{r}. \tag{C.15}$$